Astronomy & Astrophysics manuscript no. 3900djj February 5, 2008
(DOI: will be inserted by hand later)

Fundamental properties of pre-main sequence stars in young, southern star forming regions: metallicities

The Weak-Lined T-Tauri Stars

David J. James[1,6], Claudio Melo[2,3], Nuno C. Santos[4,5], and Jérôme Bouvier[1]

[1] Laboratoire d'Astrophysique, Observatoire de Grenoble, BP-53, F-38041 Grenoble, France
e-mail: david.j.james@vanderbilt.edu,Jerome.Bouvier@obs.ujf-grenoble.fr
[2] European Southern Observatory, Casilla 19001, Santiago 19, Chile
e-mail: cmelo@eso.org
[3] Departamento de Astronomía, Universidad de Chile, Casilla 36-D, Santiago, Chile
[4] Centro de Astronomia e Astrofísica da Universidade de Lisboa, Observatório Astrónomico de Lisboa, Tapada da Ajuda, 1349-018 Lisboa, Portugal
e-mail: nuno@oal.ul.pt
[5] Observatoire de Genève, 51 ch. des Maillettes, CH-1290 Sauverny, Switzerland
[6] Dept. of Physics & Astronomy, Box 1807 Station B, Vanderbilt University, Nashville, TN 37235, USA

Received July 24, 2005; accepted ?

Abstract. *Aims.* The primary motivation for this project is to search for metal-rich star forming regions, in which, stars of super-solar metallicity will be created, as hopefully, will be extra-solar planets orbiting them ! The two aims of this project are: **1:** to show that our sample stars are young, lithium rich, magnetically active and non-accreting kinematic members of their respective regions. **2:** To measure the metallicity for such members.

Methods. The échelle spectrograph together with 's 2.2m telescope, was used to obtain high resolution (R=32000) spectra for each of our *weak-lined* T-Tauri target stars. The wavelength range of the spectra is ≃ 4000 – 8000 Å.

Results. We find (pre-main sequence) model-dependent isochronal ages of the Lupus, Chamaeleon and CrA targets to be 9.1 ± 2.1 Myr, 4.5 ± 1.6 Myr and 9.0 ± 3.9 Myr respectively. The majority of the stars have Li 6707.8 Å equivalent widths similar to, or above those of, their similar mass Pleiades counterparts, confirming their youthfulness. Most stars are kinematic members, either single or binary, of their regions. We find a mean radial velocity for objects in the Lupus cloud to be $\overline{RV} = +2.6 \pm 1.8$ km s^{-1}, for the Chamaeleon & clouds, $\overline{RV} = +12.8 \pm 3.6$ km s^{-1} whereas for the CrA cloud, we find $\overline{RV} = -1.1 \pm 0.5$ km s^{-1}.

All stars are coronally and chromospherically active, exhibiting X-ray and Hα emission levels marginally less, approximately equal or superior to that of their older IC 2602/2391 and/or Pleiades counterparts. All bar three of the targets show little or no signature of accretion from a circumstellar environment, according to their positions in a J−K/H−K′ diagram.

For the higher quality spectra, we have performed an iron-line metallicity analysis for five (5) stars in Chamaeleon, four (4) stars in Lupus and three (3) stars in the CrA star forming regions. These results show that all three regions are slightly metal-poor, with marginally sub-solar metallicities, with <[Fe/H]>= -0.11 ± 0.14, -0.10 ± 0.04 & -0.04 ± 0.05 respectively.

Conclusions. A sample of stars in several nearby, young star-forming regions has been established, the majority of which is young, lithium rich, magnetically active and are non-accreting kinematic members of their respective clouds. Within the errors, each region is essentially of solar metallicity. The spectroscopic data, comprising the major complement of observational products for this project, were collected at the European Southern Observatory at La Silla, Chile, proposal ID 70.C-0507(A).

Key words. Stars: fundamental parameters – Stars: pre-main sequence – Stars: abundances – ISM: Lupus – ISM: Chamaeleon & – ISM: Corona Australis (CrA)

1. Introduction

Lithium[1] is a fragile element in the conditions experienced in stellar interiors, and is destroyed by ^{7}Li$(p,\alpha)^4$He and ^{6}Li$(p,\alpha)^3$He reactions above stellar temperatures $\approx 2.5 \times 10^6$ K (*e.g.*, Bodenheimer 1965). However, during early pre-main sequence [PMS] evolution, *age* < 5Myr, solar-type T-Tauri stars are fully convective and their central temperatures should not yet be sufficiently high to burn Li (Strom 1994). Therefore, the presence of appreciable quantities of lithium in the spectra of candidate members of young associations and star forming regions [SFRs] is a powerful criterion for rejecting field-star non-members. Observations of young stars, both with circumstellar accretion disks (the so-called *classical* T-Tauri stars [CTTS]) and without disks (*weak-lined* T-Tauri stars [WTTS]), have shown that these suppositions are generally correct with average lithium abundances of 3.1-3.2 (*e.g.*, Magazzù, Rebolo & Pavlenko 1992; Martín et al. 1992), which correlates well with the *cosmic* abundance, *i.e.*, the average meteoritic value (presumably Li un-depleted - Reeves & Meyer 1978; Anders & Grevesse 1989; Pinsonneault, Kawaler & DeMarque 1990) and the Li abundance in the interstellar medium (Ferlet & Dennefeld 1984).

Young, rapidly rotating, convective solar-type stars are capable of manifesting surface magnetic fields through the interaction of rotation, differential rotation and convective motions, ie., the dynamo process (Parker 1955, 1979). These induced magnetic fields lead to confinement and heating of plasma, the effects of which we observe as chromospheric and coronal emissions (*e.g.*, Ca II H & K, Hα & X-rays). Empirically, enhanced levels of coronal and chromospheric emission are observed in solar-type stars as their rotation rate increases (Noyes et al. 1984; Hempelmann et al. 1995), although not ad infinitum (James et al. 2000). The correlation is founded upon the fact that rapid rotation induces greater dynamo action, and hence increased magnetic field production is realized, which results in greater magnetically-induced heating.

During the last decade, the satellite has been used extensively to perform relatively large X-ray surveys for many of the young, nearby SFRs such as Orion and the Taurus-Auriga associations (*e.g.*, Alcalá et al. 1996; Grosso et al. 2000; Stelzer & Neuhäuser 2001), with the aim of detecting their members. The reasons for choosing the X-ray domain to compliment optical surveys are multi-fold. For example, while one cannot fault the effectiveness of utilizing the results of large-scale, optical spectroscopic and photometric surveys for detecting and characterizing young stellar objects in nearby SFRs, such strategies, until recently, required immense quantities of telescope allocations and user-intensive people-hours. X-ray surveys are far more rapid and efficient. This is because the *bona fide* SFR members are likely to exhibit mean X-ray luminosities far in excess of older-open cluster members or field stars of similar mass (*e.g.*, Neuhäuser et al. 1995; Stelzer & Neuhäuser 2001), and as such there is a far larger contrast in X-rays between true SFR members and background (or foreground) field star interlopers. An important caveat to be borne in mind ought to be stated. One must remember that while extremely useful, X-ray surveys of young SFRs designed to detect substantial fractions of their members, will be inevitably be weighted toward finding the most rapidly rotating and magnetic active members of these regions, and such activity surveys yield inherently biased membership samples, which are not fully representative of the evolutionary properties of the SFR as a whole.

Existing studies of metallicity in young SFRs are sparse. Padgett (1996) conducted a spectroscopic survey to measure the metallicity for a small group of T-Tauri stars in the Orion, Chamaeleon, Ophiuchus and Taurus star-forming regions. She concluded that the mean iron abundance derived for these four SFRs is roughly solar, albeit with a dispersion (error on the mean metallicity) of about 0.05-0.06 dex. Despite being very interesting, Padgett's study only included a few stars per cloud (typically 5-8 stars) which slightly weakens her conclusions. She herself comments that her results must be confirmed on the basis of a larger sample and higher S/N spectra. Some mention of a spectroscopic survey yielding metallicities for young T-Tauri stars is also made by Keller & Koerner (2003), in support of a Legacy program. However to date, no such results have been forthcoming in the literature.

Our current research project takes advantage of extant X-ray and optical surveys of young, southern SFRs so that we may investigate the stellar properties of a sample of WTTSs found within them. Our initial mission goals are simple. [**1**] To define and catalogue a subset of genuine, *bona fide* members of the parent associations. [**2**] To refine the sample further in order to flag multiple systems for separate analyses. [**3**] To ensure that the remaining single, genuine members are slowly-rotating ($\lesssim$30 km s^{-1} say). This 'clean' sample facilitates the following scientific aims.

First, to determine the metallicity of young solar-type WTTSs in different nearby SFRs. This is because recent studies have shown that stars hosting Jupiter-like planets tend to be more metal rich (by say 0.25 dex in [Fe/H]) than those star systems for which no extra-solar planets have been found (Gonzalez et al. 2001; Santos, Israelian & Mayor 2001, Santos et al. 2004). Pursuant to these metallicity measurements, our future research campaigns will be geared toward searching for, and then characterizing, extra-solar planets orbiting these young stars, focusing our search efforts on more metal-rich SFRs.

Second, a binary population can be identified for follow-up photometric campaigns, with the goal of discovering eclipsing binaries in the SFRs. Such systems would permit us to determine the intrinsic distances to each SFR and measure empirical masses directly in young, pre-main sequence star-forming environments. This will allow us to probe cluster characteristics, such as luminosity and mass functions, in a model independent way.

Send offprint requests to: D. James

[1] The 6708 Å Li feature consists of two line doublets, one pair from the ^{6}Li isotope (6707.933 & 6708.121 Å), and one from the ^{7}Li (6707.833 & 6707.932 Å) isotope (Soderblom et al. 1990). In the Sun, and meteorites, the isotope ratio ^{6}Li/^{7}Li is $\approx$ 8% (Anders & Grevesse 1989), and it is assumed that the Li abundance in the Sun, in the field and in young open cluster stars (*age* $\lesssim$1 Gyr), is dominated by the ^{7}Li isotope.

Third, if the samples are sufficiently large, we shall ascertain if there exists sufficient empirical evidence which indicates that stellar metallicity can affect the global properties of young stars, such as rotation, lithium abundance, magnetic activity manifestations and multiplicity. Such a study is invaluable if one is finally able to judge whether environment and/or initial conditions have rôles to play in controlling the evolution of stellar parameters such as angular momentum and surface lithium abundances as stars evolve onto the main sequence.

This first article of a series, outlines our initial refinement of a sample of WTTSs in several southern SFRs for which we have obtained high resolution, high-S/N, optical spectroscopic observations. A description of the observations and their reduction are detailed in § 2. A presentation of the spectroscopic results is presented in § 3 as well as the analyses we have used to eliminate SFR non-members, multiple stars and those systems which we do not, in hindsight, adjudge to be true WTTSs. A presentation and discussion of the metallicity analysis we have performed for *bona fide*, young, single, non-accreting members of each SFR is given in § 4.

2. Target Selection and Observations

WTTS catalogues for each SFRs we are studying were constructed from All-Sky Survey [ ] detections in and around these SFRs. The rotation-magnetic activity paradigm will of course play a rôle, and we thus expect our sample to be mostly probing the tail of the angular momentum distribution where the rapid rotators are situated, as well as the binary/multiple systems.

For each SFR, the WTTS sample was constructed from detections in and around the SFR to satisfy at least one of the following criteria: (**I**) those stars having spectral types of G and early−K. (**II**) those stars having visual magnitudes of 12 or brighter ; (**III**) those stars with weak signatures of infra-red excesses (and magnetic activity), *i.e.*, having Hα EWs << 10 Å ; (**IV**) those stars exhibiting substantial Li I 6707.8 Å EWs, which is indicative of youth. (**V**) those stars which are not components of multiple systems, as judged from existing kinematic data.

These criteria were chosen so that each sample has the highest probability of representing a *bona fide* set of solar-type members of the SFR, and ensuring that the stars are indeed of the weak-lined T-Tauri class without active accretion signatures. Of course, one may also utilize infra-red colours to assist in the elimination of field-star interlopers and CTTSs from the WTTS sample. This is because the WTTSs should show negligible evidence of infra-red colour excesses. Such excesses may be attributable to CTTS-like systems having retained their circumstellar accretion disks (see § 3 for further details). In the process of the current research, this analysis was not carried out until after our spectroscopic observing run, as we were unsure of the data quality status of the two Micron All-Sky Survey [2].[2] Under such a cloud of uncertainty, we thus preferred to attend the release of the 2 all-sky data release in March 2003.

Each of our WTTS candidates for each SFR was observed at high resolution using the échelle spectrograph at the coudé station of the 2.2m telescope (fork-mounted, Ritchey-Chrétien) situated at the European Southern Observatory [ESO], La Silla, Chile during the nights of 13, 14, 19 & 20 March, 2003. The observations were performed using a 79 lines mm^{-1} échelle grating and an 2K×4K CCD as detector, with 2.7 arcsec sky and target fibres. This set-up yielded a of cross-correlated ThArNe arc lines of 0.17 Å at 5500 Å, and a useful wavelength range of $\simeq$ 4000 – 8000 Å. Examples of the processed spectra in the vicinity of the Hα region of the spectrum are shown in Figure 1.

The spectra were used to obtain heliocentric radial velocities [RVs] and projected equatorial rotational velocities [$v \sin i$] by using cross-correlation techniques (Tonry & Davis 1979) in concert with high S/N, IAU RV standards and slowly rotating stars of similar spectral type to the targets, using the spectral range 5420 – 5620 Å. This spectral order yields spectra containing many metal absorption lines and little telluric contamination. Radial velocity zero points were set by reference to spectra of the IAU radial velocity standard stars HR 1829, HR 2701, HR 4540, HR 5384, HR 6349 & HR 6468. Cross-correlation of each standard star spectrum with those of the other RV standards revealed that external errors on the standard system were about 0.2 – 0.4 km s^{-1}. Random errors due to the poorer S/N of the target spectra, spectral-type mismatch between target and standard and the effects of broadening, were determined by multiple, Monte Carlo-like simulations. Errors varied from 0.2 km s^{-1} for slowly rotating stars, increasing to $\simeq$ 2 – 3 km s^{-1} for targets rotating at $\geq$ 20 km s^{-1}.

The of the cross-correlation peaks obtained with slowly rotating, inactive standard star spectra of similar spectral types to the targets, were measured to provide $v \sin i$ determinations. The standard stars were chosen to have minimal activity in the chromospheric Ca II H & K lines, with rotation periods estimated from a correlation between rotation and chromospheric activity (Rutten 1987). The relationship between of the cross-correlation peak and $v \sin i$ was calibrated by convolving the standard star spectra with limb-darkened ($\varepsilon = 0.6$) rotational broadening profiles (Gray 1992) and cross-correlating with the unbroadened templates. Random errors were calculated by multiple, Monte-Carlo-like simulations, and proved extremely sensitive to S/N and rotation.

The error simulations took the form of testing the random effects of S/N, rotation and spectral type mis-match between target and standard star spectra. In the first instance, we took a very high S/N, narrow-lined standard star spectrum and ran-

[2] This publication makes use of data products from the Two Micron All Sky Survey, which is a joint project of the University of Massachusetts and the Infrared Processing and Analysis Center/California Institute of Technology, funded by the National Aeronautics and Space Administration and the National Science Foundation.

domly degraded it to a much lower S/N (we choose S/N=5,10,20,40,50,100) many times (normally 100 lower quality spectra were created). By cross-correlating these degraded spectra with the original high-S/N spectrum and noting the variation in cross-correlation peak values, the random error due to spectral quality can be inferred. Like-wise for the effects of target rotation upon the random error budget, we followed a similar procedure as before, except in this instance, each of the degraded spectra were rotationally broadened (artificially with a Gray profile) to various rotation rates. Again, by cross-correlating suites of rotationally broadening, randomly degraded spectra against the original *clean* spectrum, line-broadening and spectral quality errors can be inferred. Finally, to estimate errors due to spectral mis-match, high quality, narrow-lined spectra of standard stars, of various spectral types, were cross-correlated against each other to catalogue variations in cross-correlation peak values.

Given that the majority of the data obtained for this programme yield spectra with a S/N $\gtrsim$50, and we obtained spectra of standard stars with spectral-types matching those of our targets, it is likely that our $v \sin i$ measurements are accurate to about 10%, down to a lower limit of 6 km s^{-1} (the instrumental resolution of is probably considerably lower, possibly as low as 2 km s^{-1}, e.g. see Santos et al. 2002; Melo, Pasquini & Medeiros 2001, however we choose a more conservative velocity limit of 6 km s^{-1}). Such conservatism does not alter the scientific conclusions resulting from this study.

For each target spectrum, we have also measured the EWs of the Hα line at 6563Å and the Li 6708Å resonance lines using both the direct integration and the Gaussian fitting methods. For the lithium region, we simply rectified the spectrum before measuring the Li I EW, and so our values include the contributions from the small Fe +CN line at 6707.44 Å, leading to measured Li I EWs that are representative of a slightly (10 – 20 mÅ) overestimated photospheric Li presence. For instance, Soderblom et al. (1993a) report that this Fe line blend has an EW = [20(B-V)$_0$ - 3]mÅ, for main sequence, solar-type stars. In the case of Hα, the normalized Hα spectrum of a minimum-activity standard star (old, Li depleted, slowly rotating stars - *viz* HD 36436 [F7V], HR 5384 [G1V], HD 65216 [G5V], HD 73256 [G8V], HD 22049 [K2V], HD 160346 [K3V] & HD 156026 [K5V]), closest in spectral type to that of each target, was shifted to each target's RV, artificially broadened to the target star's $v \sin i$ (except in those cases where $v \sin i < 10$ km s^{-1}) and subtracted from the target's normalized Hα spectrum. This procedure yields the residual Hα emission of a target star. In effect, we are removing a photospheric contribution from the stellar Hα profiles which we are measuring. These Hα residuals represent the *filling in* of the core of the Hα profile, relative to the similar-mass, standard star spectrum, which we assume to be the result of dynamo−induced chromospheric activity and/or an accretion signature if the star is of the *classical* type.

At this point several cautionary notes should be sounded. There may be systematic errors introduced in the measurement of Hα EWs using the *spectral subtraction* technique described above, however they should not be so large as to prevent us from classifying the targets as WTTSs or CTTSs. First, if the metallicity of the target is significantly different from that of the standard star, then there may be an offset between the two spectra due to a difference in the local continuum flux and in the temperature and conditions under which a specific line is formed. Second, if any part of the line contribution was formed in an optically thick region of a target star, the entire residual EW of a spectral line cannot have its origins in regions of optically thin chromospheric emission. This is because Compton scattering from more energetic photons (than the line) may contribute to the line flux, which is herein assumed to be chromospheric in origin. Third, it may be possible that these PMS stars, some with quite high rotation velocities, may have activity cycles similar to those observed on the Sun, and may be more chromospherically active during the current observing season than, say, some time in the past (on timescales of rotation periods to years). Fourth, we choose not to telluric correct the Hα profiles of the targets. The subtraction of a similar spectral-type standard star Hα profile will in essence help to mitigate this by subtracting out the telluric feature, albeit at a strength when the standard star spectrum was taken. Some differential residual telluric feature may result after spectral subtraction, however we expect that this contribution will be no more than 10 – 20mÅ. This is likely to be of the same order as the internal statistical error bars on the EW measurement (assumes 10% errors, as is common for intermediate S/N, high resolution spectra).

3. Results

The complete astrometric and photometric data ensemble for the input catalogue for each SFR is detailed in Table 1. Segregated into specific SFRs, the data presented represent the target name (col 1), its alternative name if available (col 2), its optical position taken from Digitized Sky Survey [ ] images (cols 3 & 4 - precise to $\simeq$ 1 arcsecond - RMS), the optical magnitudes, colours, mass indices in the form of V, V−I & spectral type (taken from the literature; cols 5 – 7) and their 2 JHK$'$ magnitudes and errors of any detections within 2 arcseconds of the optical positions (cols 8 – 10).

The cross-identifications and optical data sources for individual members of those regions detailed in Table 1 are thus: for the Lupus SFR they are Krautter et al. (1997 - sources) & Wichmann et al. (1997a, b), whereas for Chamaeleon regions & they are Alcalá et al. (1995), Covino et al. (1997) and Alcalá et al. (2000). We also used ID/optical data for the CrA SFR from Neuhäuser et al. (2000), and the few data we use for the Rho Oph cloud are from Martín et al. (1998).

The results of the spectroscopic kinematic analyses and a simplistic treatment of the X-ray properties of our sample stars are presented in Table 2. In the first instance, a radial velocity analysis permits one to establish firm membership constraints. Given that all the candidates are likely to be cluster members, because of the initial selection criteria for the sample (see § 2), the primary use of the RV data is thus to establish SFR membership and multiplicity for each star. In the worse case scenario, we can also establish cluster *non-membership*.

Again, to allow husbandry of all the X-ray/kinematic data for each SFR, we categorize the SFR samples in the same way as was performed in Table 1. For each target, its X-ray count rate and luminosity (for the passband of 0.1 – 2.4 keV) is catalogued in columns 2 – 3 of Table 2. The standard conversion factor, in translating X-ray count rate to X-ray flux for negligible interstellar absorption, of 6×10^{-12} erg cm^{-2} count^{-1} has been used to determine the X-ray flux of each target. Of course, the tabulated fluxes are most likely lower limits, as one would find it hard to believe that some level of absorption of X-ray flux was not taking place in the local SFR environment. X-ray luminosities, as ratios to bolometric luminosities, are provided in column 4. SFR distances are detailed in the table footnotes and bolometric corrections have been calculated for each star, as a function of spectral type, using the relationships reported by Kenyon & Hartmann (1995 - [KH95]). Interstellar reddening estimates have been used from the data given in Table 4 (see also § 3.2.1). In columns 5 & 6, we report the literature values (see Table 2 footnotes for references) of the angular momentum parameters photometric rotation period & $v \sin i$ for each target, if known. Finally, our kinematic results for each star observed during this campaign, namely the heliocentric Julian data [HJD], radial velocity and $v \sin i$, are presented in columns 7 – 9. For completeness, we also add a comments column in which we detail target RVs found in the literature and/or whether a target has been found to be a double-lined spectroscopic binary [SB2] system.

Two rapidly rotating Chamaeleon stars, RX J0850.1-7554 & RX J0951.9-7901, yielded cross correlation functions, when their spectra were cross correlated against the suite of RV standard star spectra, which appeared somewhat double-peaked – indicative of an SB2 system. These cross correlation peaks were not always well separated, nor extremely clear, and we concede that these stars may be single in nature. Their rapid rotation and/or the presence of surface star-spots may be the cause of such inhomogeneities or double-peaks in the cross correlation functions, and not because of a secondary stellar component. We label them as *SB2?* systems (possible SB2s) and urge caution in their interpretation. One star in Chamaeleon, RX J1303.5-7701, which is an RV non-member, was remarkable in that its spectrum looked like that of a hot, high mass star of early type, and is in all likelihood a background reddened giant.

The spectral analysis data relating to the Li 6708Å & Balmer Hα 6563Å lines for each SFR target are catalogued in Table 3. The target identifier and the HJD of observation are listed in columns 1 & 2, as well as the approximate signal-to-noise [S/N] ratio of the target's spectrum, at the nearest continuum region to the 6708Å line, in column 3. As a sanity check, we choose to measure target Li 6708Å EWs using the direct integration method and the Gaussian fitting method. These data are presented in columns 4 & 5. In all cases, these two measures are within 10% of each other. In column 6, we list our adopted Li EWs, which are based on the Gaussian fitted line EWs, and a 10% error budget. We have chosen these EWs preferentially because if an individual spectrum suffers from a nearby cosmic ray event, a Gaussian fit to the line profile is less likely to be affected (unless the cosmic ray destroys several pixels, > 5 say) than by integration. If a target has two sets of Li EW from different epochs of observation, its adopted EW is the weighted mean of the two Gaussian-fitted EWs, weighted by the S/N of each of its spectra. If there already exists an extant Li measure for a target in the literature, then it is detailed in column 7 (see RV references in Table 2 for citations). Finally, the Gaussian-fitted and direct integration Hα EWs are presented in columns 8 & 9 for the *residual* chromospheric-emission profiles we have created. Extreme chromospheric emission, rapid rotation and/or surface star-spots can deform the shape of spectral line profiles, especially ones that have contributions from magnetic heating processes. Therefore, in this instance, we choose to use the direct integration EW for the Hα line, and not the Gaussian fitting method one, to mitigate against cases where the residual emission profile is distorted. We note in passing that the observation of the Lupus star RX J1605.7-3905 yielded a visually bizarre spectrum around the Li region, and so we present only its Gaussian fitted EWs.

To attain our science goals, the primary task undertaken was to establish membership of the SFR for each WTTS candidate. Combined with the initial selection criteria of the samples, outlined in § 2, we also use several physical characteristic criteria of the targets to ensure that our sample really is representative of a ensemble of young, single WTTSs, and does not include binary members and/or field star interlopers nor stars of the classical T-Tauri class.

And so, the results section is structured thus: (**a**) a discussion of the radial velocity data is presented to establish kinematic *membership* of each SFR, either single, binary or non-member in nature; (**b**) establishing fundamental parameters for each target, such as luminosity and effective temperature, for comparison to theoretical PMS isochrones and mass tracks. An age analysis to confirm youth is performed; (**c**) a comparison of how much lithium each PMS star has in its atmosphere is made with the members of the Pleiades cluster, an open cluster of known-age ($\simeq$ 100 Myr). Such a comparison allows us to further verify that the *members* of each SFR are indeed young; (**d**) an analysis is performed for each star to show that it does **not** display considerable Hα emission nor has considerable infra-red excess, so that we can confirm that each SFR *member* is of the *weak-line* class. If a sample of stars can be created for each SFR which is able to satisfy the membership, youth and WTTS-class criteria, a metallicity study can subsequently be performed upon their spectra.

3.1. Radial Velocities:

For each of the WTTS candidates listed in Table 1, we present at least one radial velocity measure of our own (and its HJD), and indeed, in many cases two measurements. Used in concert with any extant RV measurements to be found in the literature, we feel confident that we are able to ascertain whether candidates are probable kinematic members (single or binaries) of their

respective SFRs. Of course, using this criterion, we cannot yet say whether the candidate is young or is a *weak-lined* or *classical* T-Tauri star.

The comparative use of a kinematics criterion is fortunately available from existing spectroscopic surveys of SFRs. For instance, Wichmann et al. (1999) show that the mean radial velocity for an ensemble of 49 X-ray selected, Li-rich, late-type WTTS stars in the Lupus SFR is $\overline{RV} = +2.72 \pm 1.15$ km s^{-1}. For the Chamaeleon SFRs, Colvino et al. (1997) have shown that their Li-rich, detected, WTTS stars have RVs in the range +12 <RV< +18 km s^{-1}, with a clearly defined peak in the RV histogram at $\simeq +13$ km s^{-1} (their figure 7). Moreover, the results of Walter et al. (1997) and Neuhäuser et al. (2000) show that the majority of their Li-rich T-Tauri candidate members in the Corona Australis (CrA) SFR have RVs in the range $0 \rightarrow -2$ km s^{-1}. In addition, a recent multiplicity study, by Melo (2003), of young, T-Tauri stars in several SFRs further corroborates these systemic kinematic results, as have been reported by the authors cited above. In any case, the bulk 1-d kinematic properties of the SFRs that we are studying are now reasonably well-defined.

In constructing a radial velocity histogram one can search for local peaks in the kinematic space density. Starting from the RV measurements detailed in Table 2, such an analysis is presented in Figure 2. While our data ensemble, on a region by region basis, is somewhat limited by small number statistics, it can surely not be aleatory that the three peaks in the RV distribution are coincident with the mean 1-d kinematics of the CrA, Lupus and Chamaeleon SFRs discussed above.

In fact, if one were to take the average of each star's RV measure, for each SFR, as is detailed in column 9 of Table 2, one would obtain a mean RV for objects in the Lupus cloud to be $\overline{RV} = +2.6 \pm 1.8$ km s^{-1}, for the Chamaeleon & clouds, $\overline{RV} = +12.8 \pm 3.6$ km s^{-1} whereas for the CrA SFR, $\overline{RV} = -1.1 \pm 0.5$ km s^{-1}. Such an analysis includes all stars in each SFR except for RX J1307.3-7708 (which is a probable non-member of the Chamaeleon region) and the Chamaeleon object RX J1303.5-7701. The former is an RV & photometric non-member of the Chamaeleon SFR, and is a low lithium object. The latter is an RV non-member and appears in our spectra to be of early spectral-type, and we henceforth classify RX J1303.5-7701 as a field interloper in the star field of Chamaeleon, and we shall not consider this star further. We issue a *caveat lector* for this star because it has previously been classified as a G7 star (Alcalá et al. 2000), in discord with our observations.

The majority of our observed target stars are most likely *bona fide* kinematic members of their respective SFRs. Of course, while we were only able to record one or two epochs of velocities for the SB2s, the RVs of their constituent components appear to straddle the mean RV of their respective associations, indicating to us that they have a reasonable probability of being members. For the two Rho Oph stars, the only real inference that we can make is that their two single-epoch RV measures are consistent with each other. In any case, these two Rho Ophiuchus stars have infra-red colours consistent their being *classical* T-Tauri stars, and we do not consider them further (see below).

3.2. Stellar Luminosity, Lithium Depletion and Stellar Youth:

To discriminate against field star interlopers having radial velocities matching those of the parent SFR under study, thus mimicking true SFR members, one useful characteristic we can exploit is stellar age (*c.f.,* § 1). In judging stellar youth for our sample, we consider two analyses; ( ) comparison of targets' stellar luminosity-effective temperature data and theoretical stellar models on an Hertzsprung-Russell diagram [HRD]. ( ) comparison of targets' lithium content with that of a cluster of known age.

3.2.1. An Hertzsprung-Russell Diagram:

Determination of fundamental stellar parameters for each SFR target has been achieved by converting observational parameters such as magnitudes and spectral types to luminosity and effective temperature using statistically-large observational samples of Galactic field stars and theoretical stellar models. Such data for each SFR candidate, where known, are tabulated in Table 4. Effective temperatures and bolometric corrections have been calculated for each star, as a function of spectral type, using the relationships reported by KH95. Interstellar reddening is calculated by comparing target V−I colours (or in five cases, their J−H colours) to KH95 theoretical colours derived from spectral type. The SFR distances adopted for the luminosity calculations are the same as those cited in Table 2.

Bolometric luminosities, as a fraction of solar luminosity, and effective temperatures for each SFR target have subsequently been plotted on an HRD, which is shown in Figure 3. Solar metallicity (with an initial deuterium abundance of 4.5×10^{-5}), pre-main sequence isochrones and mass tracks, computed by D'Antona and Mazzitelli (1997), are also plotted. By comparison to these theoretical models, we have determined a stellar mass and age for each target star, for which we were able to determine a luminosity. Such fundamental data are reported in last two columns of Table 4.

Reassuringly, with the exception of a small handful of stars, the majority of the SFR candidate members have isochronal ages considerably younger than 20 Myr. In fact, for the Lupus, Chamaeleon & and CrA SFRs, the mean isochronal ages are 9.1 ± 2.1 Myr, 4.5 ± 1.6 Myr and 9.0 ± 3.9 Myr respectively. These values agree remarkably well with those summarized by Rebull, Wolff & Strom (2004 - their table 2) and Neuhäuser et al. (2000).

3.2.2. Detection of Lithium:

In further assessing the youthfulness for the stars comprising the SFR samples presented in Table 1, we compare the adopted lithium EWs for each target, as are detailed in Table 3, with similar spectral-type members of the 100-Myr Pleiades open cluster. The results of such a comparison are presented in Figure 4. For an effective temperature scale, we now use the spectral type-temperature relationships described in de Jager & Nieuwenhuijzen (1987) because they published temperature data for both dwarf and giant luminosity classes, thus permitting an estimate of temperature errors. One should further note that the Li I EWs for the observations have *not* been corrected for the troublesome and contaminating Fe line in the blue wing of the Li I line, at 6707.44Å. This should be of no great import to our results, since for a K2 star, its magnitude is of order 15 mÅ and is smaller than the measurement error of the main Li I line for the majority of our targets. Serving as an internal verification, and to reassure ourselves of our line measurement quality, we compare the lithium EWs we have derived with those of other authors for any target stars in common between our sample and those to be found in the extant literature. Such a comparison is graphically presented in Figure 5. For all except two or three data points, the agreement between our equivalent width system and those to be found in the literature is really rather good ($\simeq$ 34mÅ). There are two objects with really quite discordant values, namely, the Rho Ophiuchus star RX J1627.1-2419 and the Chamaeleon star RX J0951.9-7901 (the latter is a suspected SB2 system which may be a mitigating factor).

All targets in the sample, with the exception of the early-type star in the Chamaeleon sample − RX J1303.3-7701, contain a clearly defined, and in most cases substantial, Li I 6707.8Å line in their spectra. However, the most striking feature of the Li data presented in Figure 4 is that the majority of the target stars have lithium EWs considerably higher than their similar-mass (*i.e.*, similar effective temperature) Pleiades counterparts. In fact, their data points appear to lie higher even than the upper envelope to the Pleiades Li-mass distribution. Lacking a precise effective temperature scale for WTTSs, as well as proper atmospheric models, we do not attempt to derive Li abundances from the measured Li EWs. Nevertheless, that most WTTSs of our sample have larger Li EWs than Pleiades late-type dwarfs of similar temperature indicates that they are probably considerably younger than the Pleiades, and thus qualify as young, SFR candidate members (Martín, Magazzù & Rebolo 1992; Martín et al. 1994). If their RVs are in agreement with the systemic velocities of each respective SFR, they must be considered probable *young* members of each SFR, and as such, are not background or foreground field stars rambling through the Galaxy.

There are however three exceptions. The Chamaeleon & stars RX J1307.3-7708, RX J1233.5-7523 & RX J1140.3-8321 exhibit lithium EWs comparable, or even below, their similar-spectral-type counterparts in the 100-Myr Pleiades cluster. Moreover, within the error bars, the latter two stars have Li EWs in agreement with previously published values.

Understanding the case of RXJ1307.3-7708 is facile. The star is an RV non-member and its 2 JHK′ magnitudes are far too dim for it to be an unobscured WTTS member of the Chamaeleon SFR. This object is most likely a non-member of the Chamaeleon SFR. The status of the other two low-lithium stars is less obvious. Both are RV members and have 2 JHK magnitudes which are comparable to similar spectral-type stars in the SFR (although, see below). Using lithium content for RX J1233.5-7523 & RX J1140.3-8321 as an indicator of extreme youth (compared to the Pleiades), with Li I EWs of 135 & 198 mÅ respectively, it becomes clear from Figure 4 that these stars would have to exhibit effective temperatures of > 6000 K to satisfy the criterion of being substantially younger than the Pleiades. With published spectral-types of K1 and K3/4, such is not the case. These stars are potentially older stars than the Pleiades.

However, as we have already seen, their placement on an HRD yields PMS isochronal ages for these stars of 0.5 and 2.0 Myr respectively. Their absolute status is for the present time uncertain, however we retain them as photometric, kinematic and isochronal members of the Chamaeleon complex, albeit being apparently low-Li stars. Both stars are included in the metallicity analysis, see § 4 and Table 6, yielding values similar to the remainder of the Chamaeleon sample, further hinting at their *bona fide* SFR membership.

3.3. Infra-red Colour and Balmer Emission:

Some discrimination between a SFR's WTTSs and CTTTs can be probed, by plotting the candidates' 2 JHK′ data in the form of a two-colour J−H vs H−K′ diagram. Those candidates with clear infra-red excesses can thus be flagged as likely CTTS candidate members of their SFR.

By exploiting the 2 data for each star in each SFR, as are detailed in Table 1, we have investigated just such an effect in order to convince ourselves that each sample of young stars that we have observed spectroscopically is indeed a *bona fide* set of WTTSs, and not of the CTTS class. A two colour infra-red diagram using data for our WTTS candidates is plotted in Figure 6. Also shown are similar data for a sample of single, classical T-Tauri stars in Orion, as identified by Neuhäuser et al. (1995), and a sample of nearby, F→M, main sequence, field stars identified by Nidever et al. (2002). All data are taken from the 2 all-sky release catalogue of March 2003. We include for completeness a J-H/H-K' relation for the intrinsic colours of field dwarfs and giants as detailed by Bessel & Brett (1988), transformed onto the 2 JHK′ system (Carpenter 2001).

Reassuringly, all bar three of the WTTS candidates of these SFRs lie close to the field-star population in J−H/H−K′ space, indicating that most of these young, T-Tauri stars are indeed of the *weak-lined* class and not of the *classical* one. The three exceptions are for the Chamaeleon star RX J1112.7-7637 and the two Rho Ophiuchus candidates. The 2 data for these

stars indicate that they are more reddened objects or have infra-red excesses higher than those seen for any of the other WTTS candidates in our sample, with colours more representative of the Orion CTTS distribution. In fact, the Rho Ophiuchus star RX J1627.1-2419 appears to be highly reddened, at the Av≃ 5 level. As such, we cannot have faith in the photospheric purity of this Chamaeleon spectrum and the two Rho Ophiuchus ones, in lieu of the fact that their spectra may have contributions from a circumstellar component or be suffering from higher-than expected reddening. We shall therefore not consider them further in any of our analyses, including the metallicity one. It is interesting to note in passing, that the $v \sin i$ value we obtain for the apparently extincted Chamaeleon star is about three times faster than the value published in the literature.

One could also argue the point that there are three or four other target stars in our sample showing some very small level of infra-red discrepancies (≃ 0.1 magnitudes). Their 2 data place them just above the shoulder of the Bessel & Brett intrinsic colour curve for dwarfs, and are potentially situated along the Bessell & Brett intrinsic giant-star sequence. These stars are identified as the Chamaeleon objects RX J1129.2-7546, RX J1140.3-8321, RX J1158.5-7754a & RX J1159.7-7601. The one star in this group whose JHK′ data place it furthest away from the Bessel & Brett dwarf curve, some 0.1 magnitudes in H-K′ colour, is RX J1140.3-8321 – an RV member of the association; It is also one of the low-lithium stars identified in § 3.2.2.

In order to be sure that some CTTSs are not contaminating our metallicity sample, we have also measured the residual Hα emission in each of the targets. A perusal of the direct integration EW data for the Hα line, in Table 3, shows that only one object has an Hα EW > 2.5Å, RX J1625.6-2613, considerably below the canonical limit of 10Å for a star to be classified as a *classical* type T-Tauri star. This Rho Ophiuchus star is already flagged as a possible CTTS (or very reddened object), as inferred from its position in the two-colour J-H/H-K′ diagram. Simply stated, in terms of Hα emission, only this star does not appear to be of the WTTS class.

3.4. Magnetic Activity and Rotation:

The X-ray activity for our WTTS sample is shown graphically in Figure 7, in which X-ray luminosity, as a fraction of bolometric luminosity, is plotted against spectroscopic rotation rate. To enable an estimate and comparison of the X-ray activity levels, similar data are also plotted for single, solar type members of the 30-50 Myr IC 2602 & IC 2391 clusters. Given that the WTTSs exhibit Lx/Lbol values comparable, as a function of rotation rate, to the older clusters, we assume that this X-ray activity is coronal in nature.

It is clear that members of the IC clusters have attained maximal Lx/Lbol values, approaching a plateau or *saturation*-like level of 10^{-3}, as is observed for solar-type members of main sequence clusters such as the Alpha Per and Pleiades (Randich et al. 1996; Stauffer et al. 1994). This *saturation* in X-ray level is independent of rotation rate. However, while we ascertain that the target WTTSs are indeed extremely X-ray active, their Lx/Lbol values appear to be at a level $\simeq 2-3$ times weaker than their IC 2391/2602 counterparts. This maximal level of Lx/Lbol emission among the WTTSs appears to be plateau-like, and moreover appears independent of rotational velocity. Furthermore, for $v \sin i < 30$ km s^{-1}, there is a quite considerable dispersion in X-ray emission among the WTTSs, at the 0.5 dex level.

The case for analysis of the Hα emission is similar to the X-ray one. A photospheric contribution has already been subtracted from each WTTS, allowing us the freedom to discuss a true chromospheric contribution to the line, at least for those stars where we are sure there is little or no *classical*-like circumstellar contribution. A comparison to the older Pleiades cluster is possible because Soderblom et al. (1993b) have published Hα EWs (and rotation rates) for solar type stars, determined in an identical manner to the one presented herein; that is to say, where a photospheric Hα profile has already been subtracted on a star-by-star basis for each Pleiad.

A graphical representation of such data is presented in Figure 8, where residual emission Hα EWs are plotted against spectroscopic rotation rates for the WTTSs and their Pleiad solar-type counterparts. There are three striking features; (**a**) The WTTSs are indeed chromospherically active at a similar, or indeed higher, level than the 100 Myr Pleiades stars. (**b**) As is the case for X-ray emission, there appears to be an emission plateau, albeit less well defined than the X-ray one, at about 1.5 – 2.0 Å, which is more or less independent of rotation rate. (**c**) At any given rotation rate, there is considerable scatter about the *mean* residual Hα emission level.

4. Metallicities

4.1. Stellar parameters and chemical analysis

Using our spectra, we have derived stellar parameters and metallicities using the same methodology used by Santos, Israelian & Mayor (2004). In the first instance, EWs for a list of 39 Fe and 16 Fe lines were measured using a Gaussian fitting procedure within the IRAF task. The line-list used is an upgrade of the list presented in Santos et al. (2004), with the addition of 4 more Fe lines taken from the literature (see Table 5). As before, the $\log gf$ values for the added lines were computed from an inverted solar analysis using solar EWs measured from the Kurucz Solar Atlas (Kurucz, Furenlid & Brault 1984), and a Kurucz grid model for the Sun having [$T_{\rm eff}$, $\log g$, $\xi_{\rm t}$, $log\epsilon_{Fe}$] = 5777K, 4.44 dex, 1.00 km s^{-1}, 7.47 dex.

The spectroscopic analysis was done in LTE using the 2002 version of the code (Sneden 1973)[3], and a grid of Kurucz 9 atmospheres (Kurucz 1993). The atmospheric parameters for our program stars were obtained from the Fe and Fe lines by iterating until the correlation coefficients between $\log\epsilon$(Fe) and χ_l, and between $\log\epsilon$(Fe) and $\log(W_\lambda/\lambda)$ were zero, and the mean abundance given by Fe and Fe lines were the same. This procedure, using iron ionization and excitation equilibrium, was shown to give excellent results for solar-type dwarfs. The results of our analysis are presented in Table 6, together with the number of Fe and Fe lines used in each case, and the for each set of lines.

At this point, an interesting digression allows us to compare stellar effective temperatures, derived from photometric and spectroscopic analyses, for target stars common to lithium abundance sample (see § 3.2.2) and the metallicity one. We examine the temperatures derived using spectral type-temperature relationships described in de Jager & Nieuwenhuijzen (1987), and for those determined using an Fe-line ionization and excitation equilibrium analysis (see Table 6). The results of such a comparison are plotted in Figure 9. There is a general, broad-range agreement ($\sim$ 225 K) between the two temperature systems, however, there are also three or four targets with quite different photometric and spectroscopic temperatures (at the $>$ 300K level). It is possible that the spectral types for these stars, the Chamaeleon objects RXJ 1201.7-7859 & RXJ 1233.5-7523 and the CrA star RXJ 1839.0-3726, are incorrect by a sub-class or two, and yet we find no evidence for excessive photometric reddening in these stars nor are their lithium EWs low (except for RX J1233.5-7523) nor Hα emission levels particularly high.

The errors on the atmospheric parameters were derived as in the same manner as that presented in Gonzalez & Vanture (1998). Since the around the average abundance given by the Fe lines is used to compute the final uncertainties in the [Fe/H] abundance (instead of the $/\sqrt{n}$, with n being the number of lines used), it may be that these errors are slightly overestimated.

The relatively low S/N ratio of our spectra (always below $\sim$100), together with the fact that most of our targets are cool K-dwarfs (with small Fe lines), makes our metallicity analysis difficult and in a few cases impossible. In all, we could only obtain satisfactory stellar parameters for 12 WTTSs in our entire sample. Furthermore, only for a very few stars rotating faster than $\sim$15 km s^{-1} could we measure the line EWs, although these include most of the initial targets. In these cases, however, the results must be viewed with caution, as line-blending for rapid rotators can severely limit the precision of the EW measurements and hence the metallicity results.

The micro-turbulence velocities [V_t] we have derived are detailed in Table 6, and are considerably above the ones found for main-sequence dwarfs with similar temperature (see *e.g.*, Santos et al. 2004). This may be due to the effect of magnetic fields, as discussed in Steenbock & Holweger (1981 - however, see also discussion in Padgett 1996).

Recently, Morel et al. (2004) have studied the detailed effects of stellar spots affecting the determination of stellar parameters and metallicity for RS CVn stars. Their results show that the final abundances are indeed affected, although not always strongly, by the presence of photospheric spots. This issue may thus have particular importance when studying young, magnetically stars like the ones in our sample. These effects may in part explain the metallicity dispersion observed in stars belonging to the same SFR (see also next section). Unfortunately, the quality of our spectra and the relatively large error bars we calculate for our derived [Fe/H] results hinders any clear and productive discussion of the effect of photospheric inhomogeneities on metallicity determinations.

Finally, in our analysis we have considered that our target stars do not have any significant spectroscopic veiling. At this stage, this is a reasonable supposition because as the 2 photometry data indicate, our data ensemble in each SFR is dominated by stars of the *weak-lined* class (Hartigan, Edwards & Ghandour 1995). Small amounts of low-level veiling could however be responsible for some representation of the dispersion in the derived [Fe/H] values.

4.2. The metallicity of the Star Formation Regions

In total we have obtained metallicity determinations for 12 WTTS stars in 3 different SFRs: Five objects in Chamaeleon (Cha), four in Lupus (Lup), and three in Corona Australis (CrA).

In Table 7 we present the average and of the metallicity values computed, considering all the stars with [Fe/H] values measured in each SFR, as well as taking only those stars with projected rotational velocity values $v \sin i < 15$km s^{-1}. As mentioned above, stars with larger $v \sin i$ values will have higher uncertainties for their derived stellar parameters and metallicities; these indeed usually present the largest deviations from the mean [Fe/H] (see Table 6).

In all cases, the average metallicity obtained for each SFR is below solar, typically in the range 0.0 to -0.2 dex. This is in agreement with the results from X-ray studies of SFRs (e.g., Pallavicini, Franciosini & Randich 2004). X-ray observations, however, sample the stellar corona, where the abundances do not reflect the real photospheric abundances (see *e.g.*, review by Audard 2004). Given that the peak in the metallicity distribution of stars in the solar neighbourhood is also below solar (*e.g.*, Allende Prieto et al. 2004; Taylor & Croxall 2005; Santos et al. 2005), the metallicities we derive for these relatively nearby SFRs maybe not be such a surprise.

Globally, the relatively small dispersion in the [Fe/H] values for a given SFR attest to the quality of our measurements. The results are clearly below the derived error bars in the individual [Fe/H] estimates, suggesting that these latter may be overestimated

[3] The code 2002 can be downloaded at http://verdi.as.utexas.edu/moog.html

(see previous section). Also, the small dispersion gives us confidence that the use of the sample WTTSs we have targeted may be indeed a good indicator of the metallicity for each of the study regions.

Padgett (1996) have also derived stellar metallicities for stars in the Cha SFR. The average metallicity they have derived for their five objects is -0.06 ± 0.14, a value that is compatible with the CrA results listed in Table 7.

5. Summary

Using high-resolution spectra of X-ray selected, WTTS candidate members of the Lupus, Chamaeleon & and CrA star forming regions, we have established kinematic membership of their parent associations, proved that these stars are young, confirmed that each is of the *weak-line* class of T-Tauri star and is magnetically active. These analyses have allowed us to create a sample of high quality spectra for youthful, single *bona fide* members of each region.

An analysis of radial velocities derived for WTTS candidate members in each region shows that majority of the samples are 1-d kinematic members of their parent associations. We find a mean RV for objects in the Lupus cloud to be $\overline{RV} = +2.6 \pm 1.8$ km s^{-1}, for the Chamaeleon & clouds, $\overline{RV} = +12.8 \pm 3.6$ km s^{-1} whereas for the CrA SFR, we find $\overline{RV} = -1.1 \pm 0.5$ km s^{-1}, consistent with earlier studies in these regions.

Using extant photometry and distance estimates, we have determined fundamental properties for SFR candidate members such as luminosities and effective temperatures. These parameters, used in concert with pre-main sequence theoretical stellar models, allow us to determine model-dependent isochronal ages of the Lupus, Chamaeleon and CrA targets to be 9.1 ± 2.1 Myr, 4.5 ± 1.6 Myr and 9.0 ± 3.9 Myr respectively.

The youthfulness of the stars is further confirmed by measuring Li 6707.8 Å equivalent widths and comparing them to similar data for single, solar-type members of the 100 Myr Pleiades open cluster. All bar three target stars have Li EWs at or above the upper envelope of the lithium EW distribution, as a function of mass, in the Pleiades.

By comparing coronal and chromospheric activity indicators to solar-type stars in the young IC 2602/2391 (30-50 Myr) and/or Pleiades clusters, we find that the majority of our SFR targets are extremely magnetically active with L_x/L_{bol} values and Hα EWs which are almost, but not quite, as active as their maximally-active older, solar-type counterparts.

The better quality spectra of single, genuine members of each SFR are used to investigate the primary scientific question motivating this project. Are any of these star formation regions metal-rich, and can we detect a metallicity spread among their members ? Such project goals are crucial to our future studies of these regions in our efforts to detect and then characterize any extra-solar planets orbiting these young stars. To this end, for the higher quality spectra, we have performed an iron-line metallicity analysis for five (5) stars in Chamaeleon, four (4) stars in Lupus and three (3) stars in the CrA SFRs. All three regions are actually slightly metal-poor, with marginally sub-solar metallicities, with <[Fe/H]>= -0.11 ± 0.14, -0.10 ± 0.04 & -0.04 ± 0.05 respectively.

Acknowledgements. Most of this project was conducted within the framework of the European Research Training Network entitled *The Formation and Evolution of Young Stellar Clusters* (HPRN-CT-2000-00155), from which we gratefully acknowledge support. Some support has also been derived from an *career award* grant #0349075, which is also gratefully acknowledged. Support from Fundação para a Ciência e a Tecnologia (Portugal) to N.C.S. in the form of a scholarship (SFRH/BPD/8116/2002) and grant reference POCI/CTE-AST/56453/2004 is gratefully acknowledged. Our thanks and gratitude go to the staff at the European Southern Observatory, La Silla, Chile. Some sections of this project were completed during a research visit by N. Santos to the European Southern Observatory, supported by its Visitor Scientist Programme.

This research has made use of the database, operated at the Centre de Données astronomiques de Strasbourg, La France, and the Leicester Database and Archive Service at the Department of Physics and Astronomy, Leicester University, UK. The authors have been Guest Users of the Canadian Astronomy Data Centre, which is operated by the Herzberg Institute of Astrophysics, National Research Council of Canada. This publication makes use of data products from the Two Micron All Sky Survey, which is a joint project of the University of Massachusetts and the Infrared Processing and Analysis Center/California Institute of Technology, funded by the National Aeronautics and Space Administration and the National Science Foundation. This research has also made use of 's Astrophysics Data System.

DJJ would also like to thank Mrs Judith Pryer for much love and support during this work, and her continued positive influences. Je veux remercier ma petite be-draggled hag, Jude, pour son amour et soutien. Elle est l'etoile la plus brilliante dans ma vie. DJJ gratefully acknowledges the hospitality of Alan & Irene Constable, of Keivan Stassun & Gina Brissenden, and of Sara & Søren Meibom, whose warmth, kindness and homes were selflessly and freely given during several research visits to various institutions.

References

Alcalá, J.M., Krautter, J., Schmitt, J.H.M.M., Covino, E., Wichmann, R., & Mundt, R., 1995, A&AS, 114, 109
Alcalá, J.M. Terranegra, L., Wichmann, R., et al. 1996, A&AS, 119, 7
Alcalá, J.M. Covino, E., Sterzik, M., et al. 2000, A&A, 355, 629
Allende Prieto, C., Barklem, P. S., Lambert, D. L., & Cunha, K. 2004, A&A, 420, 183
Anders, E., & Grevesse, N., 1989, Geochim. Cosmochim. Acta, 53, 197
Audard, M. 2004, in proceedings of the 13th Cambridge Workshop on Cool Stars, Stellar Systems and the Sun, eds F. Favata et al.
Bertout, C., Robichon, N., & Arenou, F., 1999, A&A, 352, 574

Bessel, M.S., & Brett, J.M., 1988, PASP, 100, 1134
Bodenheimer, P., 1965, ApJ, 142, 451
Casey, B.W., Mathieu, R.D., Vaz, L.P.R. et al. 1998, AJ, 115, 1617
Carpenter, J.M., 2001, AJ, 121, 2851
Covino, E., Alcalá, J.M., Allain, S. et al. 1997, A&A, 328, 187
Cutispoto, G., Pastori, L., Pasquini, L., et al. 2002, A&A, 384, 491
D'Antona, F., & Mazzitelli, I., 1997, Memorie della Societa Astronomica Italiana, Vol 68, P.807
de Zeeuw, P. T., Hoogerwerf, R., de Bruijne, J. H. J., Brown, A. G. A., & Blauuw, A., 1999, AJ, 117, 354 (University of Arizona Press)
Ferlet, R., & Dennefeld, M., 1984, A&A, 138, 303
Franchini, M., Covino, E., Stalio, R. et al. 1992, A&A, 256, 525
Gonzalez, G., Laws, C., Tyagi, S., et al. 2001, AJ, 121, 432
Gonzalez, G. & Vanture, A. D., 1998, A&A, 339, L29
Gray, D. F., 1992, The Observation and Analysis of Stellar Photospheres 2nd edn (Cambridge: University Press)
Grosso, N., Montmerle, T., Bontemps, S., et al. 2000, A&A, 359, 113
Hartigan, P., Edwards, S., & Ghandour, L. 1995, ApJ, 452, 736
Hempelmann, A., Schmitt, J. H. M. M., Schultz, M., et al. 1995, A&A, 294, 515
Hughes, J., Hartigan , P., & Clampitt, L., 1993, AJ, 105, 571
James, D., Jardine, M., Jeffries, R., et al. 2000, MNRAS, 318, 1217
de Jager, C., & Nieuwenhuijzen, H., 1987, A&A, 17, 217
Keller, J. R., & Koerner, D. W., 2003, paper presented at Meeting #203 of the American Astronomical Meeting, Dec. 2003.0502
Kenyon, S. J., & Hartmann, L., 1995, ApJS, 101, 117 [KH95]
Krautter, R., Wichmann, R. Schmitt, J. H. M. M., et al. 1997, 123, 329
Kurucz, R. L., Furenlid, I., & Brault , J. T. L. 1984, Solar flux atlas from 296 to 1300 nm (National Solar Observatory Atlas, Sunspot, New Mexico: National Solar Observatory, 1984)
Kurucz, R. 1993, ATLAS9 Stellar Atmosphere Programs and 2 km s^{-1} grid. Kurucz CD-ROM No. 13. Cambridge, Mass.: Smithsonian Astrophysical Observatory, 1993., 13
Magazzù, A., Rebolo, R., & Pavlenko, Y. V., 1992, ApJ, 392, 159
Marraco, H.G., & Rydgren, A.E., 1981, AJ, 86, 62
Martín, E. L., Magazzù, A., & Rebolo, R., 1992, A&A, 257, 186
Martín, E. L., Rebolo, R., Magazzù, A., & Pavlenko, Ya. V., 1994, A&A, 282, 503
Martín, E. L., Montmerle, T., Gregorio-Hetem, J., et al. 1998, MNRAS, 300, 733
Melo, C. H. F., Pasquini, L., & De Medeiros, J. R., 2001, A&A, 375, 851
Melo, C. H. F., 2003, A&A, 410, 269
Morel, T., Micela, G., Favata, F., & Katz, D. 2004, A&A, 426, 1007
Neuhäuser, R., Sterzik, M.F., Schmitt, J.H.M.M. et al. A&A, 1995, 297, 391
Neuhäuser, R., Walter, F.M., Covino, E. et al. 2000, ApJS, 146, 323
Nidever, D.L., Marcy, G.W., Butler, P., et al. 2002, ApJS, 141, 503
Nordström, B., Mayor, M., Andersen, J., et al. 2004, A&A, 418, 989
Noyes, R. W., Hartmann, L. W., Baliunas, S. L., Duncan, D. K., & Vaughan, A. H., 1984, ApJ, 279, 763
Padgett, D.L. 1996, ApJ, 471, 847
Pallavicini, R., Franciosini E., & Randich, S., 2004, Memorie della Societa Astronomica Italiana, v.75, P.434
Parker, E.N., 1955, ApJ, 122, 293
Parker, E.N., 1979, Cosmical Magnet Fields: Their Origin and Their Activity (Oxford Clarendon Press)
Pinsonneault, M. H., Kawaler, S. D., & DeMarque, P., 1990, ApJS, 74, 501
Randich, S., Schmitt, J., Prosser, C. F., & Stauffer, J., 1996, A&A, 305, 785
Rebull, L. M., Wolff, S. C., & Strom, S. E., 2004, AJ, 127, 1029
Reeves, H., & Meyer, J-P., 1978, ApJ, 226, 613
Rutten, R. G. M., 1987, *PhD thesis*, University of Utrecht, Netherlands
Santos, N.C., Israelian, G., & Mayor, M., 2001, A&A, 398, 363
Santos, N.C., Mayor, M., Naef, D., et al. 2002, A&A, 392, 215
Santos, N. C., Israelian, G., & Mayor, M. 2004, A&A, 415, 1153
Santos, N.C., Israelian, G., Mayor, M., Bento, J.P., Almeida, P.C., Sousa, S.G., & Ecuvillon, A.M., 2005, A&A, 437, 1127
Shevchenko, V. S., Ezhkova, O. V., Kondratiev, V. B., & Yakubov, S. D., 1995, *Information Bulletin on Variable Stars*, 4206, 1
Soderblom, D. R., Oey, M. S., Johnson, D. R. H., et al. 1990, AJ, 99, 595
Soderblom, D. R., Jones, B.F., Balachandran, S., et al. 1993a, AJ, 106, 1059
Soderblom, D. R., Stauffer, J. R., Daniel Hudon, J., & Jones, B.F., 1993b, AJ, 85, 315
Sneden C., 1973, Ph.D Thesis: University of Texas
Stauffer, J. R., Caillault, J.-P., Gagné, M., Prosser, C. F., & Hartmann, L. W., 1994, ApJSS, 91, 625
Stauffer, J. R., Hartmann, L. W., Prosser, C. F., et al. 1997, ApJ, 479, 776
Steenbock, W., & Holweger, H. 1981, A&A, 99, 102
Stelzer, B., & Neuhäuser, R., 2001, A&A, 377, 538
Strom, S. E., 1994, in 8th Cambridge Workshop on Cool Stars, Stellar Systems and the Sun, ed. J.-P. Caillault (ASP Conference Series, San Francisco) vol 64, 211

Taylor, B.J., & Croxall, K., 2005, MNRAS, 357, 967
Tonry, J. L., & Davis, M., 1979, AJ, 84, 1511
Walter, F., Vrba, F., Wolk, S., et al. 1997, AJ, 114, 1544
Wichmann, R., Sterzik, M., Krautter, J., Metanomski, A., & Voges, W., 1997a, A&A, 326, 211
Wichmann, R., Krautter, J., Covino, E., Alcalá, J.M., Neuhäuser, R., & Schmitt, J.H.M.M., 1997b, A&A, 320, 185
Wichmann, R., Bouvier, J., Allain, S., & Krautter, J., 1998, A&A, 330, 521
Wichmann, R., Covino, E., Alcalá, J. M., et al. 1999, MNRAS, 307, 909

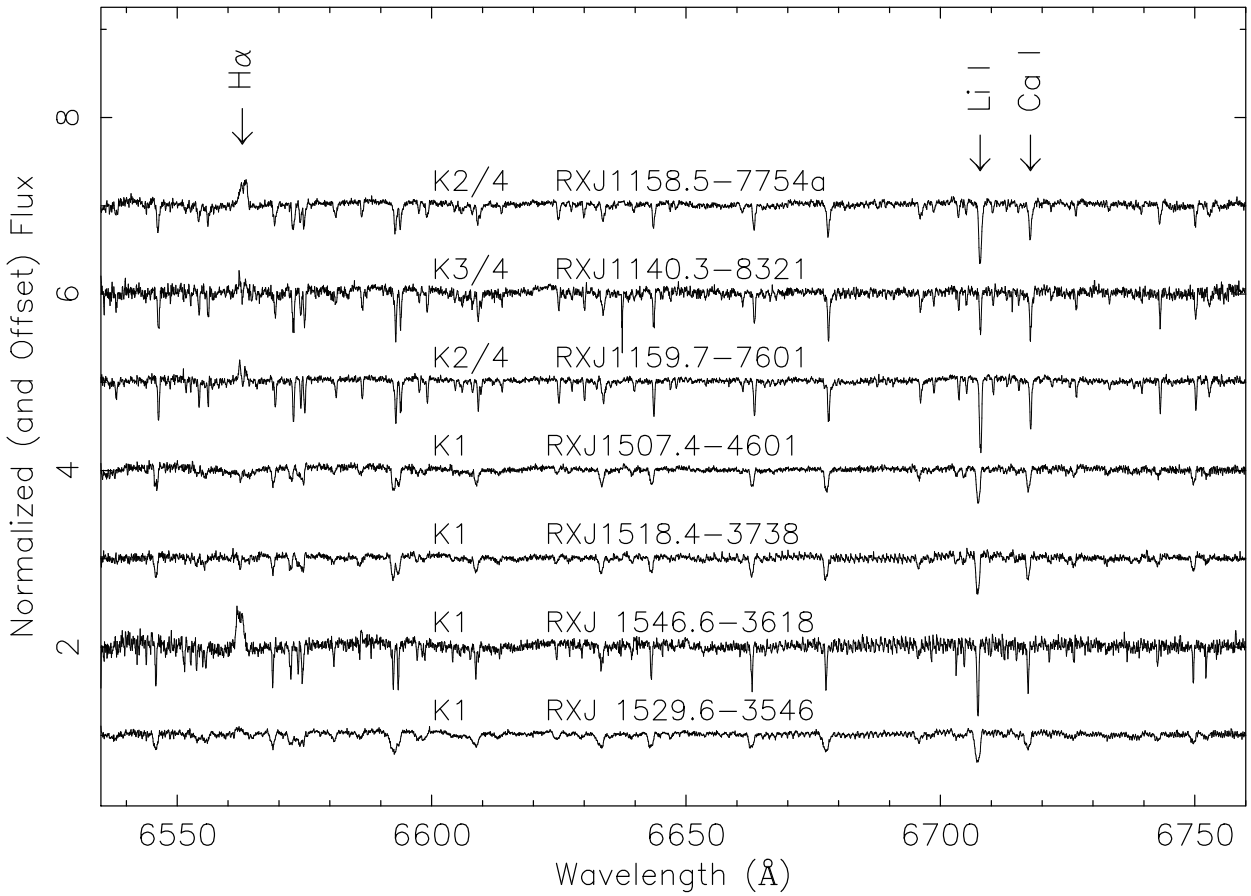

Fig. 1. Example normalized spectra are presented for a subset of the WTTS candidates in the SFRs under study. The spectra are offset for clarity. Several lines of astrophysical interest are annotated, such as the Balmer Hα line at 6562.8Å as well as the Li I (6707.8Å) and Ca I (6717.7Å) lines.

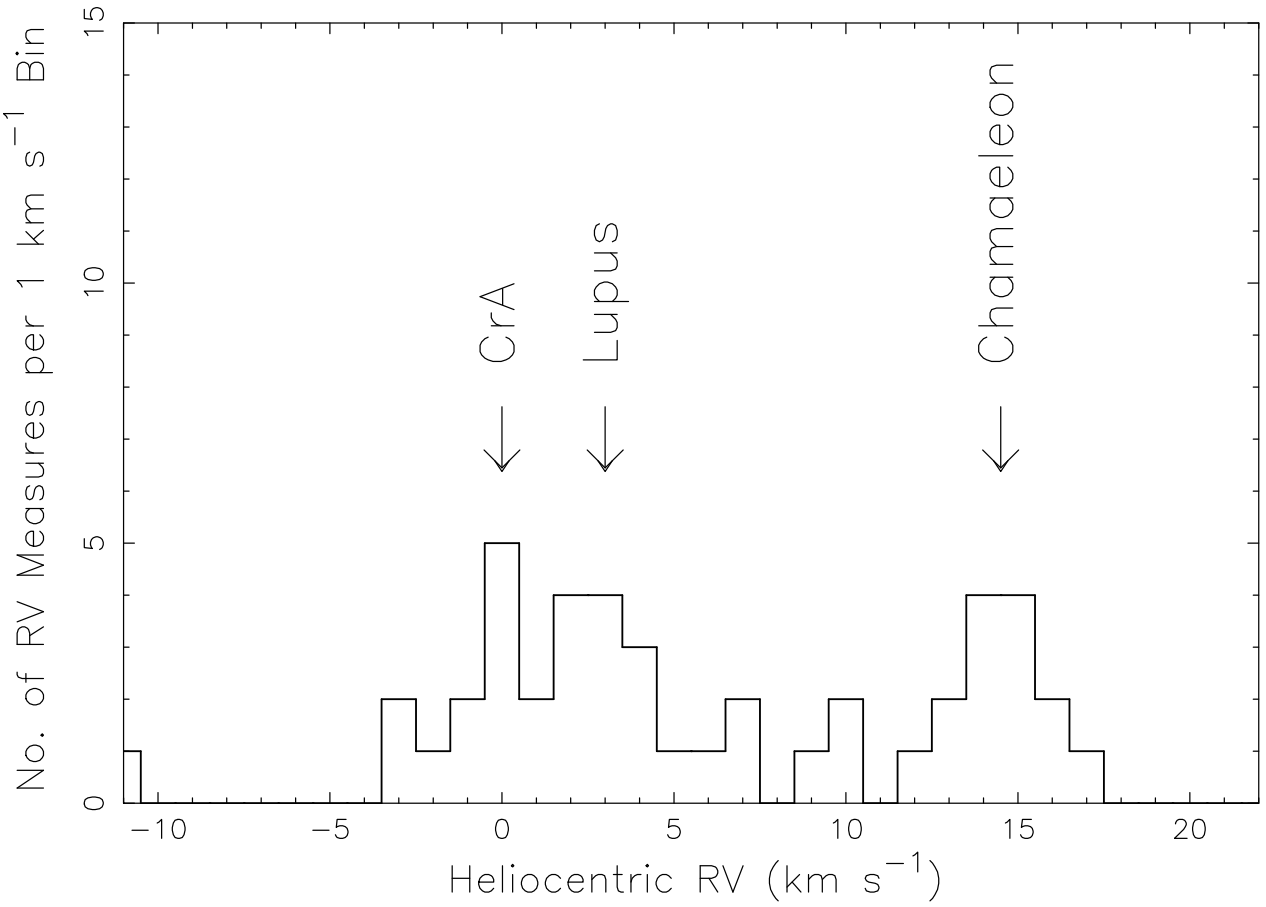

Fig. 2. An RV histogram is presented for a subset of all of the RV measurements determined during the course of this study. Peaks in the RV histogram, which are co-incident with the published cluster centric RVs of various SFRs, are labelled.

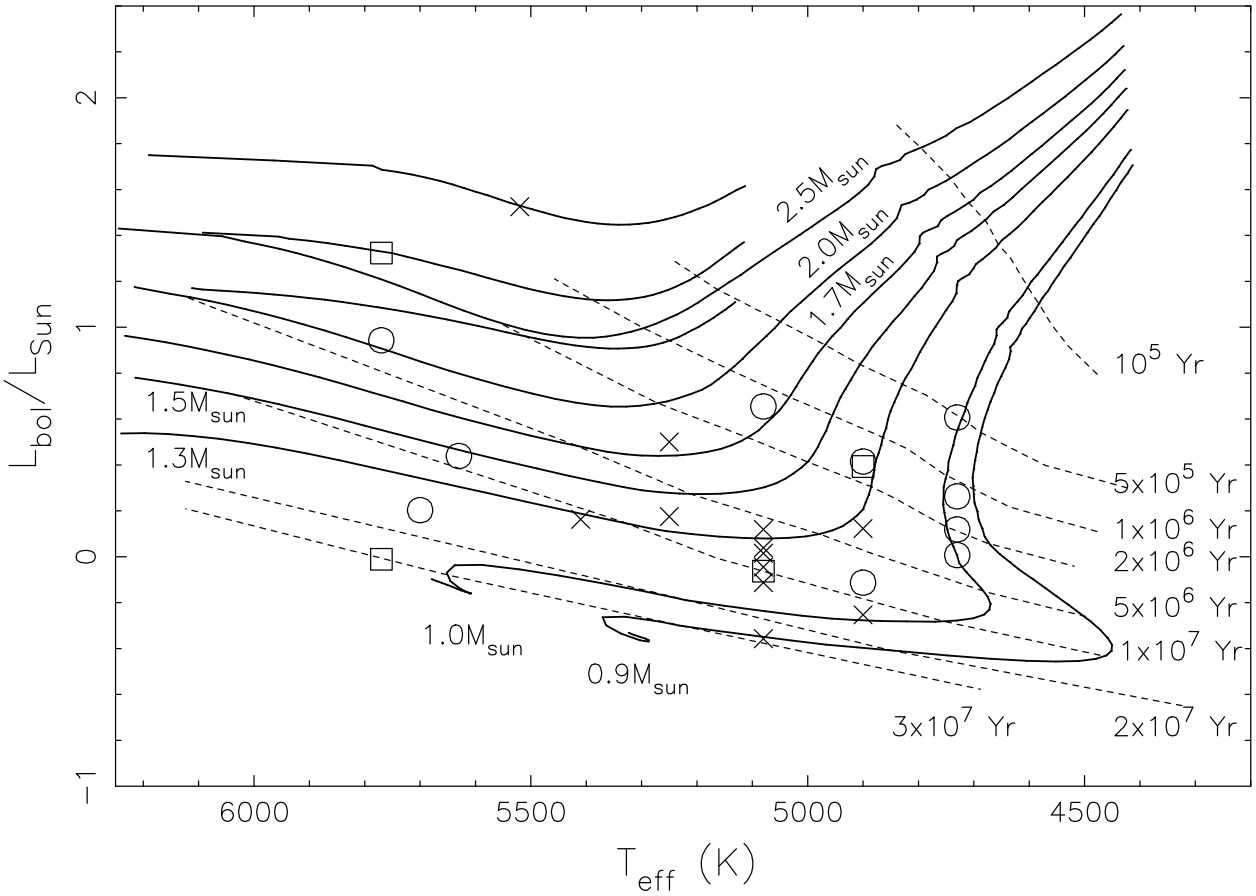

Fig. 3. An Hertzsprung-Russell diagram, which includes data points representing our target SFR candidate members, is plotted. Stellar isochrones (dashed lines) and mass tracks (solid lines) are also plotted, and are taken from the theoretical pre-main sequence, solar-metallicity stellar models of D'Antona & Mazzitelli (1997). The Lupus SFR data are depicted by the central crosses, open circles represent the Chamaeleon data, whereas the open squares are for the CrA SFR data.

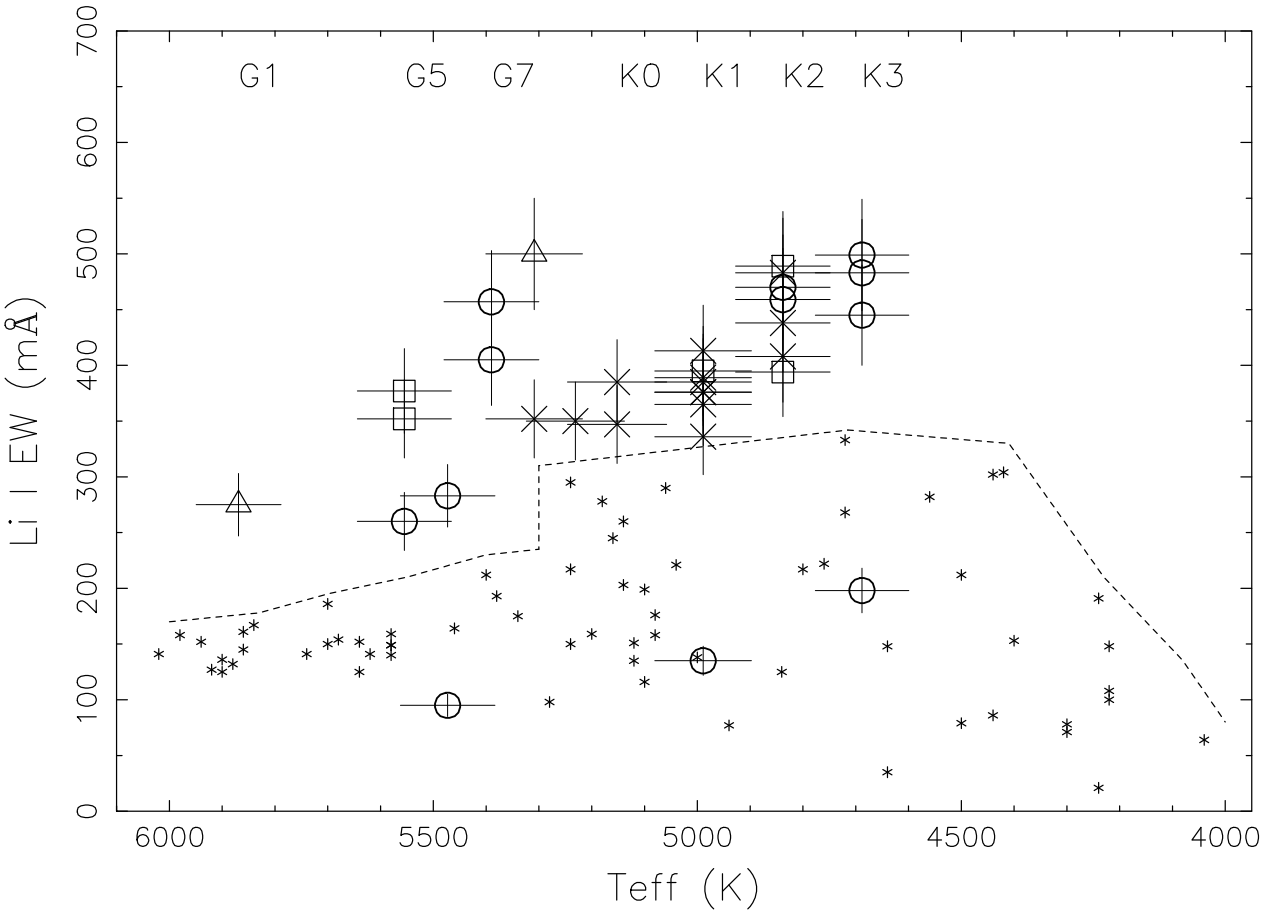

Fig. 4. The distribution of Li 6707.8 Å equivalent width versus stellar effective temperature is presented for the sample of WTTS candidates in our target SFRs, as well as for the 100 Myr Pleiades open cluster. The Pleiades data are represented as small asterisks, and are taken from Soderblom et al. (1993a). The Lupus SFR data are depicted by the central crosses, open circles represent the Chamaeleon data, open triangles represent the two Rho Ophiuchus star measurements, whereas the open squares are for the CrA SFR data. The effective temperatures for the young SFR data sample are derived (and interpolated) from a spectral-type versus temperature analysis, for luminosity class stars, performed by de Jager & Nieuwenhuijzen (1987). Errors bars on the temperatures are estimated from temperature differences between the luminosity class and class results. The hand-drawn, dashed line represents the Pleiades upper envelope of lithium equivalent widths as a function of mass.

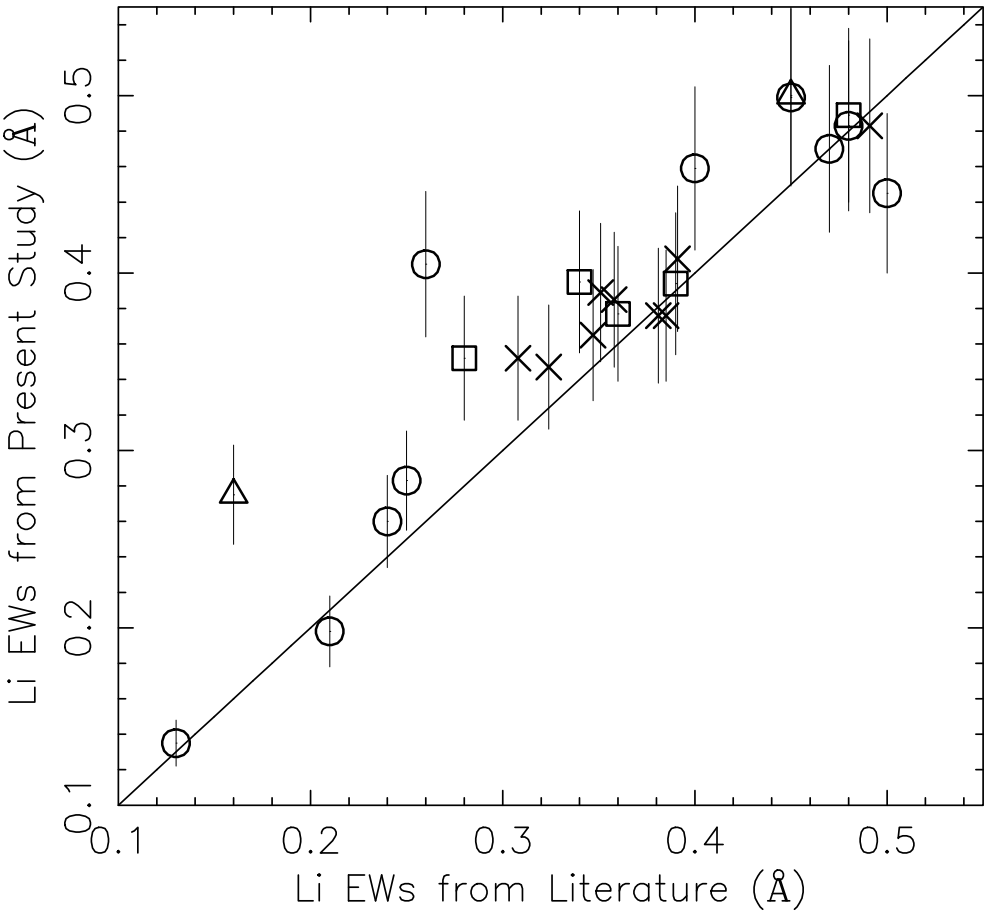

Fig. 5. A comparison between the equivalent width measurement scale of the Li 6707.8Å line for the SFRs targets in the current study is presented for the spectra we have obtained and the extant data in the literature. The symbols for the SFR data source are the same as those presented in Figure 4. The solid line is indicative of equality between our EW measurement system and those found in the literature, and is **not** a fit to the data. We note that an independent data reduction of the data for RXJ0951.9-7901 yields a lithium EW = 0.28 Å, instead of our $\simeq$ 0.4 Å result, far more in line with the value of 0.26 Å to be found in the literature. Such a discrepancy could be due to the rapid rotation and/or possible binary nature of this star.

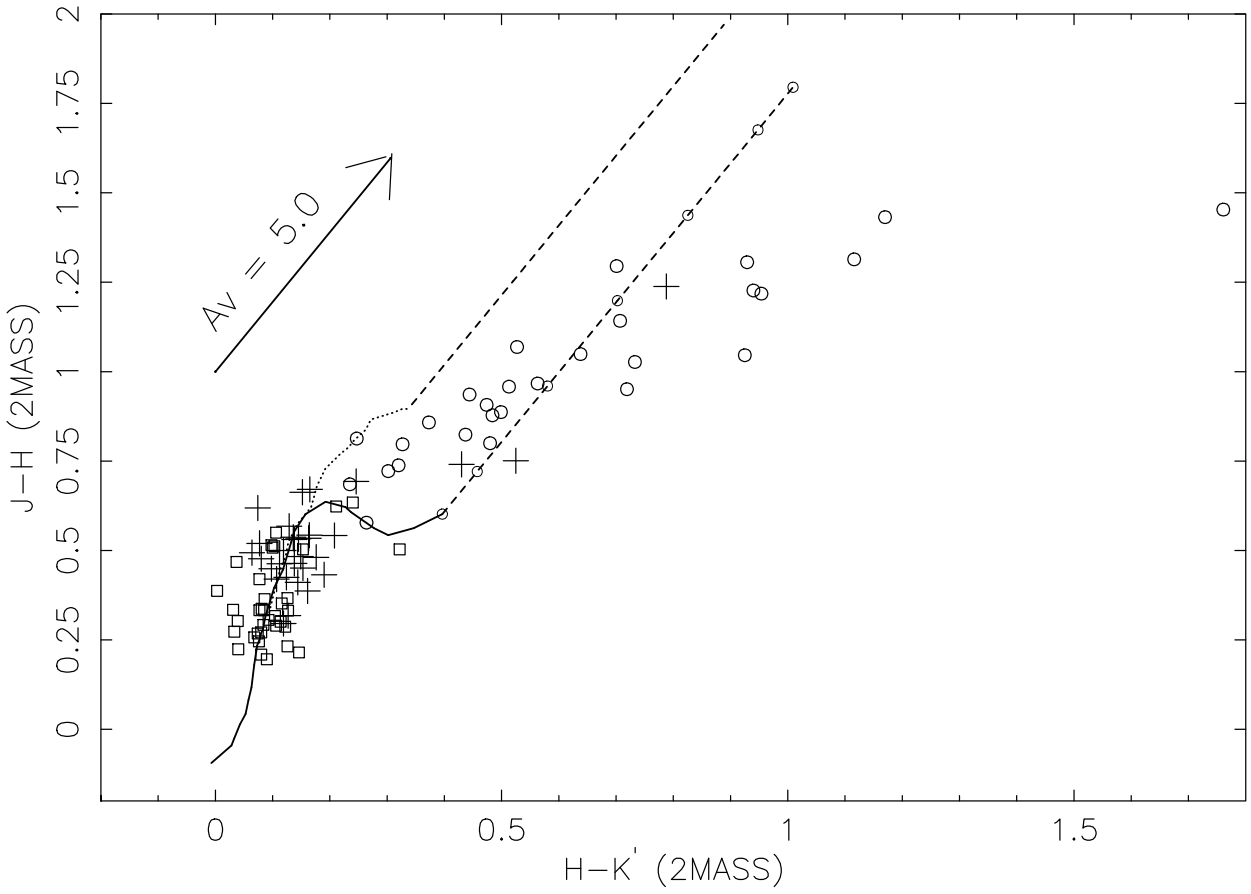

Fig. 6. A 2 J–H/H–K′ two-colour diagram is shown for the WTTS sample (crosses) detailed in Table 1. Also plotted are 2 data for a sample of single CTTSs (open circles) located in Orion (identifications taken from Neuhäuser et al. 1995) and a sub-sample of the single, F→M, main sequence, field stars (open squares) identified by Nidever et al. (2002). The solid line represents a J-H/H-K' relation for the intrinsic colours of field dwarfs as detailed by Bessel & Brett (1988), transformed onto the 2 JHK′ system, whereas the dotted line is the equivalent one for giant stars. The two dashed lines represent reddening vectors originating from the extrema of the Bessel and Brett dwarf and giant sequences.

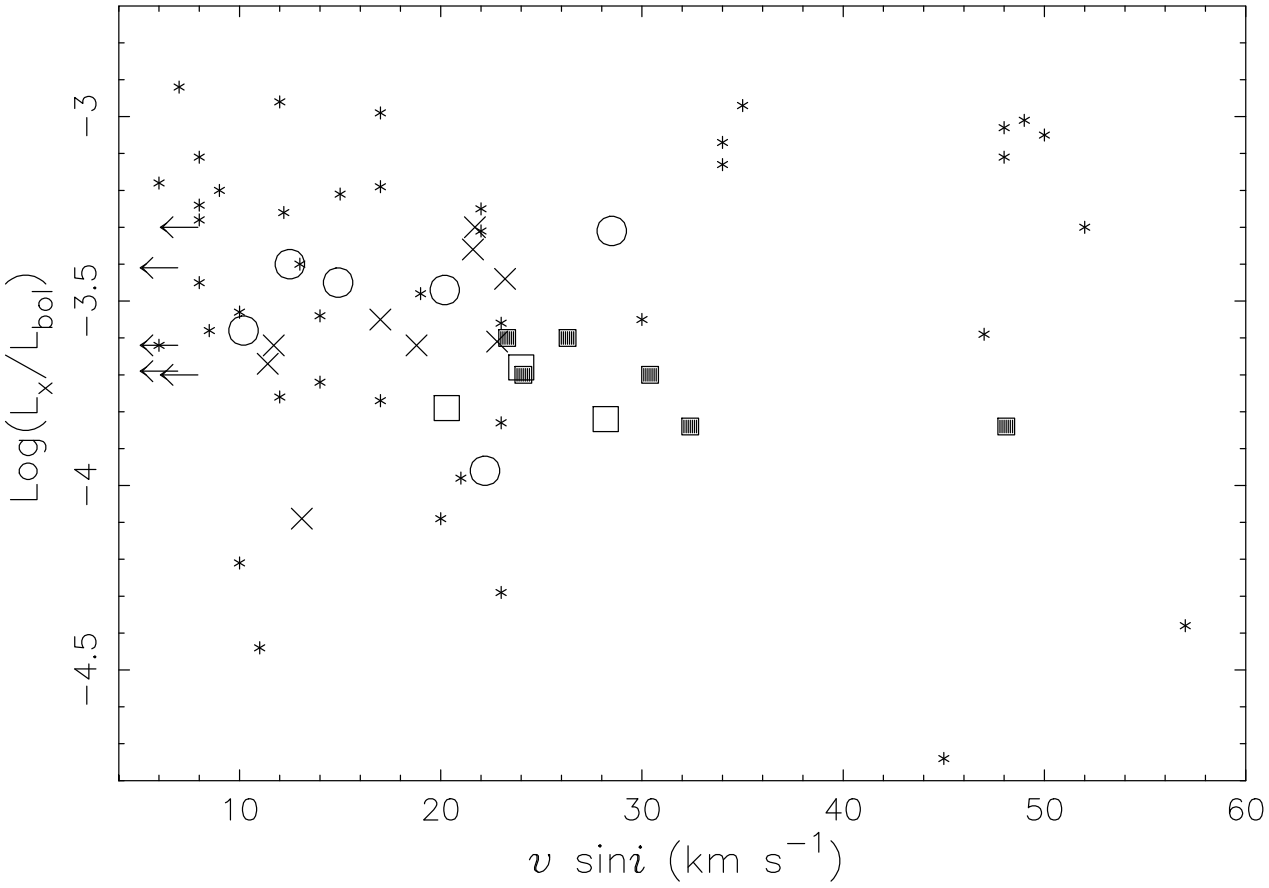

Fig. 7. X-ray luminosity, as a fraction of bolometric luminosity, is plotted against spectroscopic rotation rate for SFR candidate-members detailed in Table 2. The symbols for the SFR data source are the same as those presented in Figure 4. X-ray activity-rotation data for the SB2 stars discovered in the sample are depicted by filled squares, and given the lack of further information, we have allocated 50% of the X-ray luminosity to each component of each SB2. Also plotted for comparison, are the relevant data for a sample of single, solar-type stars in the young (30-50 Myr) IC 2391 & 2602 clusters (small asterisks - Stauffer et al. 1997).

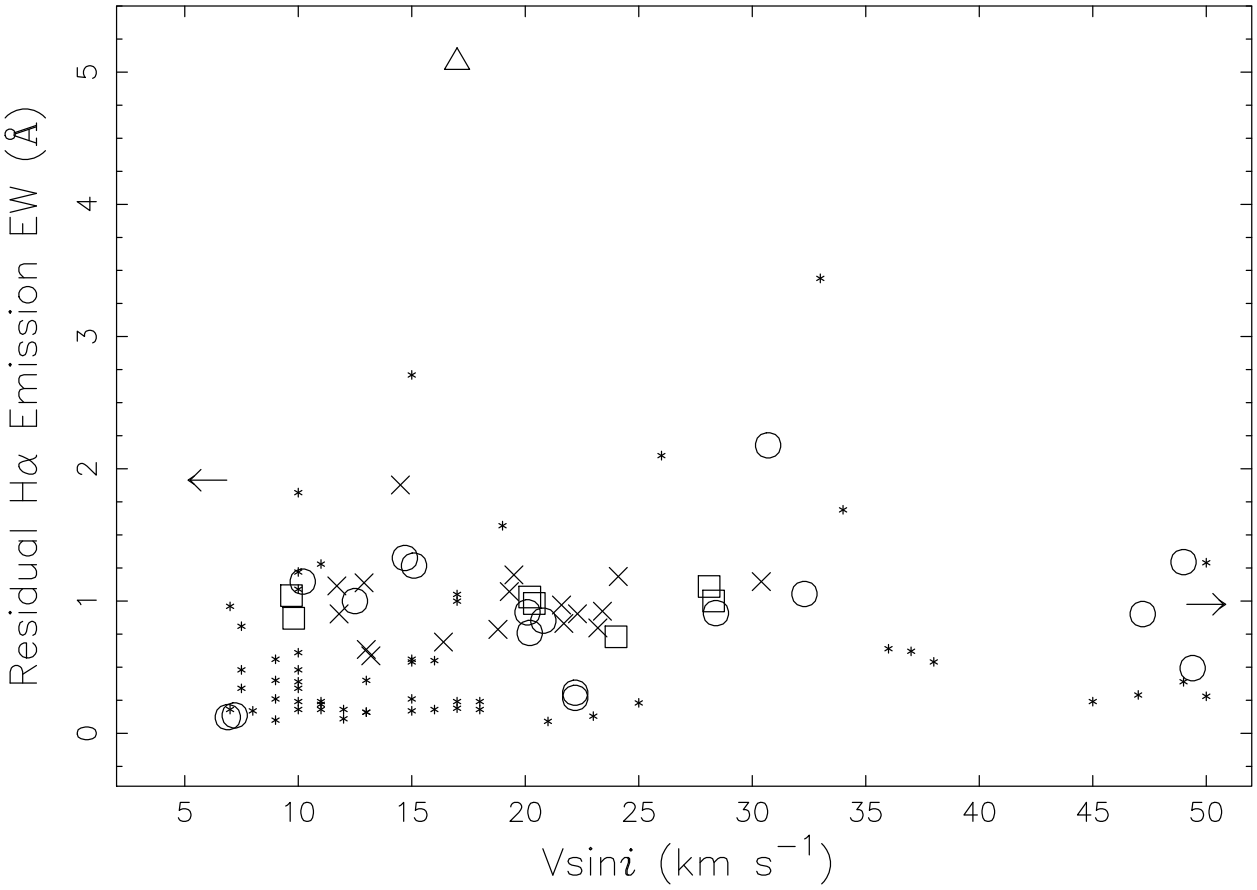

Fig. 8. The relationship between residual Hα emission strength (direct integration) and projected equatorial velocity for the WTTS candidate members of the target SFRs is presented. The symbols for the SFR data source are the same as those detailed in Figure 4. Also included are data for single, solar-type Pleiads (asterisks - data taken from Soderblom et al. 1993b).

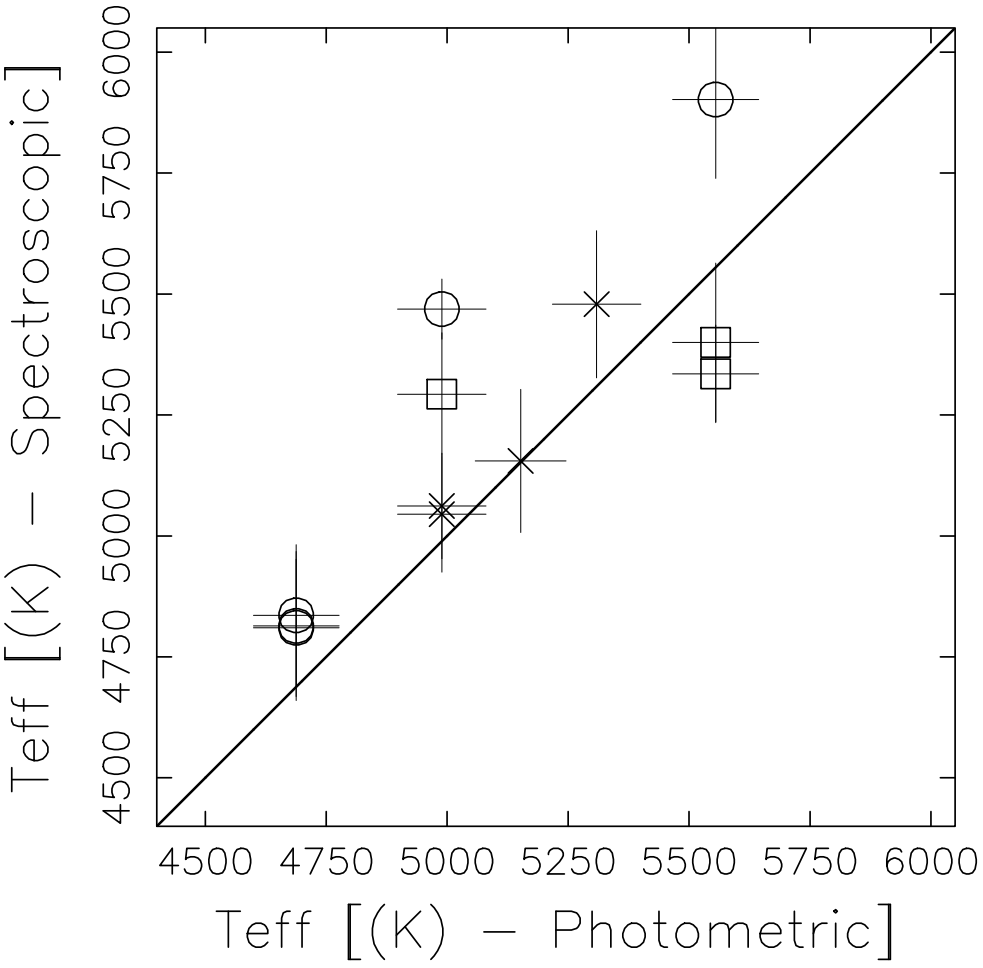

Fig. 9. A comparison between the temperature scales derived for the photometric (lithium abundance) analysis and the spectroscopic (metallicity) analysis is presented. The symbols for the SFR data source are the same as those presented in Figure 4. The solid line is indicative of equality between the two temperature systems, and is **not** a fit to the data.

Table 1. Basic astrometric/photometric data for the WTTS samples, observed spectroscopically, in each SFR .

TARGET[a]	Alt. ID	RA(2000)[b]	DEC(2000)[b]	V	V−I	Sp. Ty.	J[c] (± err)	H[c] (± err)	K′[c] (± err)
Lupus :									
RX J1507.2-3505	K 3	15 07 14.6	-35 04 58.9	10.53	1.26	K0	8.893 ± 0.021	8.416 ± 0.053	8.336 ± 0.023
RX J1507.4-4601	K 4	15 07 27.6	-46 01 06.0	11.71		K1	9.735 ± 0.024	9.284 ± 0.030	9.131 ± 0.021
RX J1515.7-3331	K 20	15 15 45.4	-33 31 59.1	10.69	1.00	K0	8.981 ± 0.022	8.461 ± 0.020	8.384 ± 0.023
RX J1518.4-3738 (V* LW Lup)	K 25	15 18 26.9	-37 38 02.5	10.92	1.01	K1	9.081 ± 0.035	8.618 ± 0.045	8.506 ± 0.021
RX J1523.4-4055 (V* MM Lup)	K 29	15 23 25.6	-40 55 46.8	11.87	1.16	K2	9.957 ± 0.023	9.389 ± 0.023	9.260 ± 0.023
RX J1524.5-3652 (V* MP Lup)	K 32	15 24 32.4	-36 52 03.3	11.30	1.01	K1	9.549 ± 0.023	9.049 ± 0.021	8.930 ± 0.019
RX J1525.0-3604	K 33	15 25 03.6	-36 04 45.8	10.92	1.09	K1	8.998 ± 0.030	8.465 ± 0.038	8.320 ± 0.022
RX J1529.6-3546 (PPM 293919)	K 42	15 29 38.6	-35 46 52.1			K1	8.788 ± 0.020	8.257 ± 0.033	8.119 ± 0.016
RX J1529.7-3628	K 43	15 29 47.3	-36 28 38.0			K2	9.643 ± 0.025	9.106 ± 0.027	8.970 ± 0.025
RX J1546.6-3618	K 70	15 46 41.0	-36 18 47.5	11.28	1.07	K1	9.490 ± 0.024	8.947 ± 0.025	8.783 ± 0.021
RX J1547.6-4018	K 73	15 47 41.8	-40 18 26.7	11.08	1.05	K1	9.294 ± 0.024	8.811 ± 0.034	8.662 ± 0.025
RX J1601.1-3320 (V* MZ Lup)	K 93	16 01 08.9	-33 20 14.1	10.88	1.07	G8	9.027 ± 0.029	8.552 ± 0.034	
RX J1605.7-3905 (PPM 747449)	K 103	16 05 45.1	-39 06 06.8	10.49	0.90	G9	8.910 ± 0.029	8.523 ± 0.045	8.362 ± 0.027
RX J1608.9-3905	K 116	16 08 54.2	-39 06 06.4	10.88	1.14	K2	8.909 ± 0.030	8.375 ± 0.047	8.212 ± 0.029
Chamaeleon & :									
RX J0850.1-7554		08 50 05.7	-75 54 38.9	10.57	0.82	G6	9.259 ± 0.026	8.848 ± 0.025	8.704 ± 0.019
RX J0951.9-7901 (HD 86356)		09 51 51.1	-79 01 38.8	10.22	0.93	G7	8.587 ± 0.032	8.138 ± 0.034	8.040 ± 0.029
RX J1112.7-7637 (CHXR 50)	HBC 588	11 12 25.0	-76 37 06.2	12.43	1.41	K0/4	9.275 ± 0.030	8.524 ± 0.055	7.999 ± 0.031
RX J1129.2-7546		11 29 13.2	-75 46 26.2	12.91	1.76	K3	9.817 ± 0.026	9.124 ± 0.021	8.878 ± 0.024
RX J1140.3-8321		11 40 17.5	-83 21 00.8	11.56	1.33	K3/4	9.328 ± 0.023	8.709 ± 0.045	8.635 ± 0.019
RX J1158.5-7754a		11 58 28.7	-77 54 29.2	10.59	1.43	K2/4	8.219 ± 0.029	7.556 ± 0.042	7.404 ± 0.021
RX J1159.7-7601		11 59 42.9	-76 01 26.0	11.30	1.37	K2/4	9.140 ± 0.027	8.469 ± 0.038	8.304 ± 0.027
RX J1201.7-7859 (HD 104467)		12 01 39.7	-78 59 16.6	8.59		G5	7.263 ± 0.027	6.967 ± 0.044	6.848 ± 0.018
RX J1233.5-7523 (HD 109138)		12 33 30.6	-75 23 11.5	9.47		K1	8.201 ± 0.020	7.883 ± 0.040	7.756 ± 0.040
RX J1239.4-7502		12 39 21.8	-75 02 38.9	10.24	1.06	K2/3	8.434 ± 0.021	7.953 ± 0.033	7.777 ± 0.021
RX J1303.5-7701 (CHIIXR24)		13 03 31.3	-77 01 53.7			G7			
RX J1307.3-7708 (CHIIXR35)		13 07 15.2	-77 07 51.0			G6	12.004 ± 0.023	11.584 ± 0.024	11.477 ± 0.025
Rho Ophiuchus :									
RX J1627.1-2419		16 27 10.3	-24 19 12.3			G1	8.745 ± 0.027	7.507 ± 0.038	6.719 ± 0.024
RX J1625.6-2613		16 25 38.5	-26 13 53.4			G8	8.688 ± 0.019	7.947 ± 0.055	7.517 ± 0.024
CrA SFR :									
CrAPMS 2 (V* V702 CrA)	HBC 678	19 02 01.9	-37 07 42.9	10.44	0.93	G5	8.903 ± 0.018	8.478 ± 0.042	8.354 ± 0.027
RX J1839.0-3726	NWC-13	18 39 05.1	-37 26 20.5	10.81	1.00	K1	9.075 ± 0.021	8.581 ± 0.029	8.517 ± 0.023
RX J1853.1-3609 (HD 174656)	NWC-55	18 53 05.9	-36 10 22.8	9.60		K2	7.905 ± 0.023	7.473 ± 0.049	7.283 ± 0.020
RX J1917.4-3756 (SAO 211129)	NWC-135	19 17 23.8	-37 56 49.5	9.90		K2	8.217 ± 0.029	7.675 ± 0.049	7.467 ± 0.029
CrAPMS 4SE		18 57 20.7	-36 43 00.3	10.95	1.00	G5	9.271 ± 0.024	8.807 ± 0.033	8.669 ± 0.023

a – Nomenclature based on Rosat All-Sky Survey detections. [http://www.xray.mpe.mpg.de/cgi-bin/rosat/rosat-survey]

b – Astrometric data determined from Digitized Sky Survey images. [http://cadcwww.dao.nrc.ca/cadcbin/getdss#1]

c – JHK data taken from the 2 All-Sky Release Point Source catalogue (March 2003). [http://pegasus.phast.umass.edu/2mass.html]

Table 2. An X-ray and kinematic data ensemble for each star detailed in Table 1.

TARGET	X-ray[a,b,c] ct rate [ct s^{-1}]	Log L_x^d [erg s^{-1}]	Log (L_x/ L_{bol})	P_{rot} [days]	$v \sin i$ [km s^{-1}]	HJD (+2450000)	RV [km s^{-1}]	$v \sin i$ [km s^{-1}]	Comments[e]
Lupus :									
RX J1507.2-3505	0.07 ± 0.02	29.99	-4.09		15.0	2713.762	+2.1	13.0	RV = +1.4
						2718.766	+2.2	13.2	
RX J1507.4-4601	0.06 ± 0.02	29.93	-3.30			2718.790	+6.9	21.7	
RX J1515.7-3331	0.10 ± 0.02	30.15	-3.61	2.28	25.0	2713.860	+1.1	22.3	
						2718.925	+1.9	23.4	
RX J1518.4-3738	0.13 ± 0.02	30.26	-3.36	2.98	25.0	2718.746	+3.7	21.6	RV = +3.7
RX J1523.4-4055	0.037 ± 0.012	29.71	-3.62	4.15	9.9	2719.769	+5.6	11.7	RV = +6.8
RX J1524.5-3652	0.06 ± 0.02	29.93	-3.55	2.91	19.0	2713.826	+4.4	16.4	RV = +4.2
						2719.792	+4.6	17.6	
RX J1525.0-3604	0.13 ± 0.02	30.26	-3.44			2718.852	+4.8	23.2	
RX J1529.6-3546	0.11 ± 0.02	30.19				2718.879	+16.4	19.3	SB2
						2718.879	−11.3	19.5	SB2
RX J1529.7-3628	0.06 ± 0.02	29.93				2719.715	+3.2	14.5	
RX J1546.6-3618	0.05 ± 0.02	29.85	-3.69		7.1	2713.705	+7.2	≤ 6	RV = +2.5
						2719.747	+7.3	≤ 6	
RX J1547.6-4018	0.06 ± 0.01	29.93	-3.67		10.0	2713.737	+3.1	11.8	RV = +2.8
						2718.916	+3.2	12.9	
RX J1601.1-3320	0.10 ± 0.02	30.15	-3.62	3.78	21.9	2713.799	+2.3	18.8	RV = +3.0
RX J1605.7-3905	0.16 ± 0.02	30.35	-3.40			2713.780	+2.2	> 50	
RX J1608.9-3905					~ 49	2718.900	+9.7	30.4	RV = −0.6
						2718.900	−25.8	24.1	SB2
Chamaeleon &									
RX J0850.1-7554	0.17 ± 0.02	30.68	-3.30		45	2712.590	+17.1	49.4	RV = +15.5
						2718.521	+35.0	26.5	SB2?
						2718.521	−0.8	23.3	SB2?
RX J0951.9-7901	0.17 ± 0.02	30.68	-3.54		73	2712.620	+39.8	49.0	RV = +12.2
						2712.620	−20.3	32.6	SB2?
						2718.533	+38.1	47.2	SB2?
						2718.533	−35.1	32.3	SB2?
RX J1112.7-7637	0.08 ± 0.02	30.36	-3.31		11	2712.694	+13.6	30.7	RV = +16.0
						2718.546	+15.2	28.4	
RX J1129.2-7546					20	2713.628	+15.9	20.8	RV = +11.4
						2719.528	+15.5	19.9	
RX J1140.3-8321	0.11 ± 0.02	30.50	-3.40		13	2718.563	+14.0	12.5	RV = +10.5
RX J1158.5-7754a	0.30 ± 0.04	30.93	-3.45		11	2713.656	+10.4	15.1	RV = +13.1
						2718.614	+10.1	14.7	
RX J1159.7-7601	0.10 ± 0.02	30.46	-3.58		10	2718.636	+15.1	10.2	RV = +13.1
RX J1201.7-7859	0.20 ± 0.02	30.76	-3.96		21	2712.734	+12.3	22.2	RV = +10.0
						2718.678	+13.6	22.2	RV = +22.3
RX J1233.5-7523					7	2712.760	+14.8	7.2	RV = +14.0
						2718.716	+16.0	6.9	RV = +15.1
RX J1239.4-7502	0.19 ± 0.02	30.72	-3.47		19	2713.675	+14.5	20.2	RV = +13.1
						2718.726	+14.2	20.1	
RX J1303.5-7701						2712.779	−121.1		Early-Type
RX J1307.3-7708						2712.794	−25.3	≤ 6	

a The standard conversion factor, for negligible interstellar absorption, of 6×10^{-12} erg cm^{-2} $count^{-1}$ has been used.

b These fluxes are lower limits, as it is unlikely that these stars represent a sample of unabsorbed X-ray emitters (see text).

c For the ROSAT passband 0.1 – 2.4 keV.

d Distances used for luminosity calculations: Lupus, d=140 pc (Hughes et al 1993; Bertout, Robichon & Arenou 1999; de Zeeuw et al. 1999); Chamaeleon, d=160 pc (Bertout et al. 1999; Rebull et al. 2004 and references therein); CrA SFR, d=120 pc (Morraco & Rydgren 1981; Casey et al. 1998).

e Lupus Vsini/Periods/RV data are taken from Wichmann et al. (1998, 1999); Chamaeleon Vsini/RV data are taken from Covino et al. (1997), Cutispoto et al. (2002) & Nordström et al. (2004); CrA SFR Vsini/RVs/Period data are taken from Neuhäuser et al. (2000), Franchini et al. (1992), Walter et al. (1997) & Shevchenko et al. (1995).

TARGET	X-ray[a,b,c] ct rate [ct s^{-1}]	Log L_x^d [erg s^{-1}]	Log (L_x/ L_{bol})	P_{rot} [days]	$v \sin i$ [km s^{-1}]	HJD (+2450000)	RV [km s^{-1}]	$v \sin i$ [km s^{-1}]	Comments[e]
Rho Ophiuchus :									
RX J1627.1-2419						2712.852	−2.7		
RX J1625.6-2613						2712.886	−3.5	17.0	
CrA SFR :									
CrAPMS 2	0.08 ± 0.02	29.93	-3.79	2.79	20	2713.909	−0.7	20.2	RV = −2.2, −1.2
						2719.923	0.0	20.4	RV = −2.6
RX J1839.0-3726					17.8	2719.869	−1.6	9.8	RV = −4.8
RX J1853.1-3609	0.19 ± 0.04	30.28	-3.68			2719.837	−3.2	24.0	
RX J1917.4-3756	0.19 ± 0.03	30.28	-3.82			2713.920	−0.9	28.1	
						2719.817	+0.5	28.3	
CrAPMS 4SE					< 10	2719.901	−1.9	9.7	RV = −2.0

Table 2 Cont/d.

Table 3. A spectral-line data ensemble, for each star detailed in Table 1, is presented for the Li 6708Å & Balmer Hα 6563Å lines .

TARGET	HJD (+2450000) [days]	S/N[a]	Li 6707.8 EW [Å] (INT[b])	Li 6707.8 EW [Å] (GF[c])	Li 6707.8 EW [Å] (ADP[d])	Li 6707.8 EW [Å] (LIT[e])	Hα EW [Å] (GF[c])	Hα EW [Å] (INT[b])
Lupus :								
RX J1507.2-3505	2713.762	50	0.319	0.330	0.347 ± 0.035	0.324	0.622	0.634
	2718.766	74	0.350	0.351			0.553	0.586
RX J1507.4-4601	2718.790	62	0.326	0.336	0.336 ± 0.034		0.637	0.831
RX J1515.7-3331	2713.860	77	0.376	0.410	0.385 ± 0.038	0.358	0.871	0.904
	2718.925	80	0.353	0.364			0.745	0.923
RX J1518.4-3738	2718.746	90	0.352	0.365	0.365 ± 0.037	0.347	0.673	0.970
RX J1523.4-4055	2719.769	22	0.399	0.408	0.408 ± 0.041	0.391	1.057	1.115
RX J1524.5-3652	2713.826	34	0.375	0.402	0.389 ± 0.039	0.351	0.809	0.690
	2719.792	36	0.377	0.379				
RX J1525.0-3604	2718.852	82	0.372	0.385	0.385 ± 0.039		0.648	0.797
RX J1529.6-3546	2718.879	92	0.401	0.413	0.413 ± 0.041		0.672	1.072
	2718.879						0.754	1.198
RX J1529.7-3628	2719.715	25	0.443	0.438	0.438 ± 0.044		1.518	1.878
RX J1546.6-3618	2713.705	39	0.372	0.376	0.376 ± 0.038	0.381	1.605	1.914
	2719.747							
RX J1547.6-4018	2713.737	38	0.390	0.395	0.376 ± 0.037	0.385	0.717	0.903
	2718.916	67	0.368	0.374			0.768	1.138
RX J1601.1-3320	2713.799	68	0.348	0.352	0.352 ± 0.035	0.308	0.822	0.786
RX J1605.7-3905	2713.780	43		0.350	0.350 ± 0.035		0.721	0.976
RX J1608.9-3905	2718.900	100	0.455	0.483	0.483 ± 0.049	0.491	0.593	1.147
	2718.900						0.721	1.186
Chamaeleon &								
RX J0850.1-7554	2712.590	87	0.248	0.278	0.283 ± 0.028	0.25	0.497	0.493
	2718.521	62	0.265	0.300				
	2718.521							
RX J0951.9-7901	2712.620	98	0.353	0.405	0.405 ± 0.041	0.26	0.857	1.295
	2712.620							
	2718.533	72	0.397	0.457	0.457 ± 0.046		0.661	0.902
	2718.533						0.650	1.054
RX J1112.7-7637	2712.694	64	0.452	0.482	0.470 ± 0.047	0.47	1.707	2.178
	2718.546	49	0.414	0.435			0.693	0.909
RX J1129.2-7546	2713.628	27	0.484	0.497	0.499 ± 0.050	0.45	0.804	0.852
	2719.528	11	0.527	0.570				
RX J1140.3-8321	2718.563	64	0.195	0.198	0.198 ± 0.020	0.21	0.893	1.000
RX J1158.5-7754a	2713.656	65	0.495	0.501	0.483 ± 0.048	0.48	1.384	1.268
	2718.614	87	0.473	0.478			1.150	1.326
RX J1159.7-7601	2718.636	90	0.430	0.445	0.445 ± 0.045	0.50	0.892	1.147
RX J1201.7-7859	2712.734	100	0.252	0.259	0.260 ± 0.026	0.24	0.313	0.307
	2718.678	160	0.246	0.260			0.283	0.268
RX J1233.5-7523	2712.760	81	0.151	0.144	0.135 ± 0.013	0.13	0.142	0.136
	2718.716	95	0.127	0.130			0.132	0.122
RX J1239.4-7502	2713.675	81	0.426	0.436	0.459 ± 0.046	0.40	0.660	0.759
	2718.726	82	0.452	0.480			0.771	0.915
RX J1303.5-7701	2712.779							
RX J1307.3-7708	2712.794	8	0.082	0.095	0.095 ± 0.010			

a Approximate S/N of nearest continuum region to the blaze centre of the Li I 6708 Å order.

b EWs measured using direct integration between the limits of where the Li I /Hα feature approaches unity on either side of its central absorption/residual emission feature.

c EWs measured using a Gaussian fit, with the same wavelength limits as for the direct integration method.

d Adopted Li I 6708Å EW, using weighted mean of the Gaussian fitted EWs for targets having spectra recorded on different observing nights. Errors levels are estimated to be 10%.

e Li I 6708Å EWs for these targets as reported in the extant literature.

TARGET	HJD (+2450000) [days]	S/N[a]	Li 6707.8 EW [Å] (INT[b])	Li 6707.8 EW [Å] (GF[c])	Li 6707.8 EW [Å] (ADP[d])	Li 6707.8 EW [Å] (LIT[e])	Hα EW [Å] (GF[c])	Hα EW [Å] (INT[b])
Rho Ophiuchus :								
RX J1627.1-2419	2712.852	14	0.222	0.275	0.275 ± 0.028	0.16	0.559	1.208
RX J1625.6-2613	2712.886	42	0.512	0.500	0.500 ± 0.050	0.45	4.287	5.075
CrA SFR :								
CrAPMS 2	2713.909	98	0.334	0.353	0.352 ± 0.035	0.28	0.987	1.031
	2719.923	46	0.315	0.329			0.711	0.982
RX J1839.0-3726	2719.869	45	0.385	0.395	0.395 ± 0.040	0.34	0.692	0.870
RX J1853.1-3609	2719.837	58	0.378	0.394	0.394 ± 0.040	0.39	0.592	0.730
RX J1917.4-3756	2713.920	93	0.471	0.490	0.489 ± 0.049	0.48	1.049	1.110
	2719.817	48	0.457	0.472			0.747	1.001
CrAPMS 4SE	2719.901	51	0.372	0.377	0.377 ± 0.038	0.36	0.584	1.041

Table 3 Cont/d.

Table 4. Fundamental stellar parameters, and the intermediate data used to calculate them, are presented for each SFR candidate member. Mass and Age estimates are derived by comparison of their luminosity-temperature data with the theoretical models and tracks computed by D'Antona and Mazzitelli (1997).

TARGET	V	V−I	Sp. Type	V−I[a] KH95	J−H[a] KH95	E^{b}_{V-I} or E_{J-H}	Av[c] [mags]	B.C.[d] [mags]	T^{d}_{eff} [K]	log($L_{bol}/L_{\odot}$)[e]	Mass [$M_{\odot}$]	Age [Myr]
Lupus :												
RX J1507.2-3505	10.53	1.26	K0	0.85		0.41	1.02	-0.31	5250	0.500	1.8	3.0
RX J1507.4-4601	11.71		K1	0.93	0.47	0.00	0.00	-0.37	5080	-0.357	0.9	28
RX J1515.7-3331	10.69	1.00	K0	0.85		0.15	0.37	-0.31	5250	0.175	1.4	8.0
RX J1518.4-3738	10.92	1.01	K1	0.93		0.08	0.20	-0.37	5080	0.039	1.2	6.5
RX J1523.4-4055	11.87	1.16	K2	1.01		0.15	0.37	-0.42	4900	-0.253	1.0	14
RX J1524.5-3652	11.30	1.01	K1	0.93		0.08	0.20	-0.37	5080	-0.113	1.1	12
RX J1525.0-3604	10.92	1.09	K1	0.93		0.16	0.40	-0.37	5080	0.119	1.3	6.0
RX J1529.6-3546			K1	0.93				-0.37	5080			
RX J1529.7-3628			K2	1.01				-0.42	4900			
RX J1546.6-3618	11.28	1.07	K1	0.93		0.14	0.35	-0.37	5080	-0.045	1.2	8.5
RX J1547.6-4018	11.08	1.05	K1	0.93		0.12	0.30	-0.37	5080	0.015	1.2	7.0
RX J1601.1-3320	10.88	1.07	G8	0.81		0.26	0.64	-0.25	5520	1.525	> 2.5	< 1.0
RX J1605.7-3905	10.49	0.90	G9	0.83		0.07	0.17	-0.28	5410	0.163	1.3	11
RX J1608.9-3905	10.88	1.14	K2	1.01		0.13	0.32	-0.42	4900	0.123	1.3	4.0
Chamaeleon &												
RX J0850.1-7554	10.57	0.82	G6	0.77		0.05	0.12	-0.22	5700	0.203	1.2	17
RX J0951.9-7901	10.22	0.93	G7	0.79		0.14	0.35	-0.23	5630	0.439	1.5	8.0
RX J1112.7-7637	12.43	1.41	K0/4	1.01		0.40	0.99	-0.42	4900	-0.113	1.1	7.5
RX J1129.2-7546	12.91	1.76	K3	1.08		0.68	1.69	-0.50	4730	0.007	1.0	3.0
RX J1140.3-8321	11.56	1.33	K3/4	1.08		0.25	0.62	-0.50	4730	0.119	1.0	2.0
RX J1158.5-7754a	10.59	1.43	K2/4	1.08		0.35	0.87	-0.50	4730	0.607	1.0	0.5
RX J1159.7-7601	11.30	1.37	K2/4	1.08		0.29	0.72	-0.50	4730	0.263	1.0	1.0
RX J1201.7-7859	8.59		G5	0.76	0.36	0.00	0.00	-0.21	5770	0.943	2.1	3.0
RX J1233.5-7523	9.47		K1	0.93	0.47	0.00	0.00	-0.37	5080	0.655	1.8	0.5
RX J1239.4-7502	10.24	1.06	K2/3	1.01		0.05	0.12	-0.42	4900	0.415	1.4	2.0
RX J1303.5-7701			G7	0.79				-0.23	5630			
RX J1307.3-7708			G6	0.77				-0.22	5700			
Rho Ophiuchus :												
RX J1627.1-2419			G1	0.72				-0.19	5945			
RX J1625.6-2613			G8	0.81				-0.25	5520			
CrA SFR :												
CrAPMS 2	10.44	0.93	G5	0.76		0.17	0.42	-0.21	5770	1.323	> 2.5	< 5.0
RX J1839.0-3726	10.81	1.00	K1	0.93		0.07	0.17	-0.37	5080	-0.063	1.1	9.0
RX J1853.1-3609	9.60		K2	1.01	0.50	0.00	0.00	-0.42	4900			
RX J1917.4-3756	9.90		K2	1.01	0.50	0.04	0.35	-0.42	4900	0.393	1.4	2.0
CrAPMS 4SE	10.95	1.00	G5	0.76		0.24	0.60	-0.21	5770	-0.011	1.0 – 1.2	20.0

a Theoretical V−I or J−H values for each target's spectral type (assumes dwarf-class) are taken from KH95.

b E_{V-Ic} and E_{J-H} are calculated by subtracting the target's V−Ic or J−H colour from their theoretical values based on spectral type.

c We assume Av = 2.48×$E_{(V-I)c}$ or Av = 8.38×E_{J-H}.

d Bolometric corrections [B.C.] and effective temperatures, as a function of spectral type, are taken from KH95.

e The luminosity of the Sun is assumed to be 3.85×10^{33} erg s^{-1}.

Table 5. Addition Fe lines used in the metallicity analysis presented herein, to complement those used in an identical analysis procedure performed by Santos et al. (2004).

λ (Å)	χ_l	log gf	$EW_{\odot}$ [mÅ]
5325.56	3.220	-3.20	41.4
5414.07	3.220	-3.57	26.9
5425.25	3.200	-3.23	41.5
6456.39	3.900	-2.11	62.9

Table 6. Stellar parameters, determined from a spectroscopic metallicity analysis of Fe lines in spectra of suitable WTTS candidate members, are presented for each of the SFRs under study. The effective temperatures listed in column 8 are derived from a spectral-type versus temperature analysis (see Figure 4 and de Jager & Nieuwenhuijzen 1987).

Star	T_{eff} [K]	$\log g$ [cm s^{-2}]	V_t [km s^{-1}]	$[Fe/H]$	N (Fe , Fe)	σ (Fe , Fe)	T_{eff} [K]
			Chamaeleon				
RXJ1140.3-8321	4814 ± 154	4.07 ± 0.92	2.15 ± 0.23	−0.14 ± 0.15	23, 4	0.14, 0.51	4688 ± 177
RXJ1158.5-7754a	4810 ± 142	3.87 ± 0.51	2.11 ± 0.22	−0.26 ± 0.15	20, 2	0.13, 0.25	4688 ± 177
RXJ1159.7-7601	4836 ± 146	4.23 ± 0.33	2.07 ± 0.22	−0.18 ± 0.16	29, 6	0.16, 0.12	4688 ± 177
RXJ1201.7-7859	5902 ± 163	4.38 ± 0.43	1.99 ± 0.31	0.12 ± 0.17	14, 4	0.09, 0.18	5555 ± 178
RXJ1233.5-7523	5469 ± 62	4.40 ± 0.22	1.52 ± 0.10	−0.09 ± 0.08	35, 10	0.07, 0.10	4989 ± 183
			Lupus				
RXJ1507.2-3505	5155 ± 148	4.37 ± 0.49	2.53 ± 0.26	−0.08 ± 0.14	21, 7	0.11, 0.23	5152 ± 188
RXJ1546.6-3618	5062 ± 109	4.09 ± 0.53	2.12 ± 0.16	−0.12 ± 0.14	34, 6	0.13, 0.26	4989 ± 183
RXJ1547.6-4018	5045 ± 120	4.18 ± 0.61	2.23 ± 0.20	−0.14 ± 0.13	30, 8	0.11, 0.31	4989 ± 183
RXJ1601.1-3320	5479 ± 152	3.70 ± 0.35	2.49 ± 0.26	−0.05 ± 0.18	24, 3	0.14, 0.15	5309 ± 183
			CrA				
CrAPMS2	5400 ± 164	4.06 ± 0.45	2.41 ± 0.30	−0.09 ± 0.18	21, 5	0.13, 0.19	5555 ± 178
CrAPMS4SE	5335 ± 101	4.59 ± 0.41	2.24 ± 0.17	−0.02 ± 0.12	31, 10	0.10, 0.20	5555 ± 178
RXJ1839.0-3726	5293 ± 127	4.51 ± 0.42	2.19 ± 0.21	−0.01 ± 0.15	35, 9	0.14, 0.19	4989 ± 183

Table 7. Average and of the metallicities derived for each star formation region. N is the number of stars with [Fe/H] values in each case.

Region	N	<[Fe/H]>	
All stars			
Cha	5	−0.11	0.14
Lup	4	−0.10	0.04
CrA	3	−0.04	0.05
Stars with $v \sin i < 15$km s^{-1}			
Cha	4	−0.17	0.07
Lup	3	−0.11	0.03
CrA	2	−0.02	0.00